

Heating and Slipping Effects on Gold-Blood Flow of Nanofluid Consequent to Peristaltic Waves with Various Shape Factors in a Vertical Tube: Cancer Treatment

M. M. Ahmed¹, Essam T. Abdelwahab^{1,*}, I. M. Eldesoky^{1,2}, Ramzy M. Abumandour¹

¹ Basic Engineering Sciences Department, Faculty of Engineering, Menoufia University, Shebin El-Kom, Egypt.

² Basic Engineering Sciences Department, El-menoufia Higher Institute of Engineering and Technology, El-Menoufia.

* (Corresponding author: essam.tharwat@sh-eng.menoufia.edu.eg)

ABSTRACT

This study emphasizes the great impacts of the process of injection gold nanoparticles (AuNPs) through the blood vessels of the human body for cancer therapy. This investigation handles the effects of the heating process, the slipping, the gravity, and the various shapes of the nanosize particles on the behavior of the blood flow in a tube. The kinetics of gold-blood flow of nanofluid occurs according to the peristaltic wave which motives the flow through the body. The efficient Hamilton-Crosser model for the nanofluid thermal conductivity is selected. The governing equations of the incompressible non-Newtonian nanofluid are solved under the procedures of the perturbation strategy with a small wavenumber and long wavelength. Graphical results for the velocity, the temperature distributions, and the streamlines are deduced using MATLAB software under the effect of the heat source, Grashof number, Shapes of the AuNPs (Bricks, cylinders, and platelets), AuNPs concentrations, and slipping conditions. The results show a great impact of the heat transfer, shape factor, and the concentration of the injected AuNPs on the cancer treatment.

Keywords: Peristaltic flow; Nanofluid; Slip conditions; Shape factor; Heat transfer.

1. Introduction

In the recent four decades, cancer is one of the dangerous and fatal diseases in humans. This malignant disease is classified as the third cause of mortality worldwide [1]. Thus, the scientists and the researchers declared the war on cancer in their laboratories and researching to reduce deaths from this silent disease. The malignant tumors and neoplasms arise due to the uncontrollable growth of the body abnormal cells near their boundaries and invade the organs of the body. The metastases of the cancer cells occur when they can separate from their main tissues and invade the blood and lymph tissue to transfer to the other tissues where they are reproduced and continue in growth, these metastases finally led to death.

The main reasons for the transformation from normal cells to abnormal tumor cells are depending on the genetic factors of the persons and other external factors such as the physical, chemical, and biological carcinogens including the harmful ultraviolet radiations, infections from viruses, bacteria, or parasites, handling the aflatoxin, and the arsenic [2].

Elimination of cancer acquires many investigations and experiments [3-6] which led to many strategies for cancer therapy for instance; the conventional intervention of surgery, chemotherapy, and radiation therapy. Nanotechnology provides an excellent tool for cancer treatment as the NPs are smaller by one hundred to ten thousand times in size than the tumor cells therefore the NPs can interact within the malignant cells and proteins [7]. Photothermal therapy (PTT) is a new technique used for destruction the malignant cells by injection of the AuNPs into the blood vessels beyond the tumor tissues and exposes them to a thermal effect. The heating occurs by focusing appropriate wavelength laser pulses to the targeted AuNPs which can kill the bacteria and destroy neoplasms. The explosion of the malignant cells occurs when the AuNPs absorb the laser light and the temperature of the AuNPs reaches (70-80) oC, which is sufficient to kill and destroy them [8].

The kinetics of the gold-blood flow of nanofluid arises as a result of the peristaltic action of the smooth muscles on the tunica media of the blood vessels walls. The peristalsis has a vital role in the dynamics of many

biological fluids in the human body, e.g. the blood flow in the blood vessels of the cardiovascular, the propulsive action of the bolus via the esophagus, and the urine flow in the ureter [9-24]. Slipping at the walls may appear in certain diseases, thus the effect of slipping was taken into consideration also in the related articles [25-29]. The physical parameter Knudsen number Kn refers to the slipping case in which the flow has a tangential relative velocity at the walls and the fluid particles don't adhere on the boundaries the reasonable range is $0.01 < Kn < 0.15$, see Fang [30]. Furthermore, nanotechnology has vital contributions in the industry, chemistry, biology, engineering, medicine, and other relevant fields of research.

Nanofluids are resulting from dispersing nano-scale solid suspensions with a size range between 1 to 100 nm called NPs through the base fluid e.g. blood, oil, water, and petrol. From the medical point of view, the NPs were prepared for the treatment purpose with suitable physical characteristics. The NPs prepared in the labs from metals, oxides, or carbides. The NPs have ferromagnetic, thermal conductivities, heat transfer coefficients, and chemical properties compared to the base fluid to enhance the heat transfer and magnetic effects. Choi and Eastman [31] were the first who introduced new metallic NPs which have high thermal conductivity and were efficient in enhancing the heat transfer rate when dispersed in the base fluids. A very useful review of the different models of thermal conductivities was investigated by Kumar et al. [32]. There are several types of NPs are used in nanotechnology, for instance, gold, silver, copper, titanium, aluminum, steel, and so on [33]. The gold NPs are carefully chosen to be injected into the blood vessels for blood flow applications and particularly cancer therapy applications. The atomic number of the AuNPs is high enough to transfer the heat by natural convection which is useful for tumor PTT. The first attempt to use the AuNPs for malignant treatment was tested by Huang and El-Sayed [34] who introduced the effectiveness of the AuNPs' optical properties and in neoplasms diagnosis and PTT. Hamilton – Crosser model was a good model to express the effective thermal conductivity of the nanofluid and this model is developed with the aid of the shape factor of the NPs. There are three shapes of the AuNPs (bricks, cylinder, and platelets) each has a surface area to enhance the heat transfer by convection to the malignant tissues [35]. Researches [36, 37] handled experimentally the performance of AuNPs in the destruction of the malignancies and proved that they are safe and effective for systemic drug delivery to these malignancies.

There are only a few articles involving the interaction between NPs and the peristalsis through the different

ducts. Abdelsalam and Bhatti [38] analyzed the effect of AuNPs migration through blood flow through an endoscope. They considered the peristalsis as the motive force of the flow. They have also used the Homotopy perturbation strategy for solving the governing equations. They mentioned that cancer therapy using the AuNPs is less cost than chemotherapy and it is also a safe tool. The results showed that the increase of nanoparticle concentration and heat source enhanced the temperature distribution and eliminate the malignancy cells. The thermal and magnetic effects were applied to the peristaltic transport of the blood flow carrying out several nanoparticles to enhance the heating effect through various conduits as presented in [39-46]. Sadaf and Abdelsalam [47] dispersed two types of NPs into pure blood moving peristaltically through a tube by taking into consideration the heating effect and the shape effect of the NPs such as bricks, cylinders, and platelets. The temperature is increased by increasing the heat source parameter but increasing the Biot number reduces the temperature distribution and the tapered bolus vanished at large values of Biot number. One of the most findings was that the hybrid NPs have high performance on the heat rate better than the set NPs. Bhatti et al. [48] turned to analyze the peristaltic runoff of the gyrotactic microorganisms and the ferromagnetic NPs through the blood using Sutterby fluid model. The most accurate up to third-order perturbation strategy has been performed. The temperature distribution was large in the case of the divergent shape of the artery compared with the convergent one. The Peclet number reduced the motile microorganism curve and the non-Newtonian property opposed the flow. Abdelsalam and Bhatti [49] introduced the magnetic and thermal radiation to the peristalsis of the non-Newtonian nanofluid containing oxytocic microorganisms using the Homotopy perturbation methodology (HPM). Abdelsalam and Bhatti [50] investigated the peristaltic propulsion of the blood carrying out TiO₂ NPs in the endoscope under the influence of a variable magnetic field and a heat source. The undertaken model was Prandtl fluid model. The outcomes showed that the maximum velocity profile has existed beyond the center of the annulus. Akbar and Butt [51] have illustrated the shape factor effects on the convection heat transfer of the ferromagnetic copper water nanofluid peristaltic motion using the longwave length and small Reynolds number methodology. It was found that the increase of NPs volume fraction enhanced the thermal conductivity of the nanofluid and the shape of the platelets of NPs has the highest thermal conductivity while the shape of the bricks was the lowest. And also, the Hartmann number enhanced the velocity beyond the boundary and reduced it near to the core of the

tube. The NPs shape effects were also handled in the presence of a transverse magnetic field and the gravitational effect of the copper water nanofluid moving peristaltically. The outcomes emphasize that the temperature profile was increased by raising the NPs volume fraction with the cylinder shape, also the gravitational effect was obvious as the rise of the Grashof number led to an acceleration of the streamwise flow with high thermal buoyancy force for the shape of the platelets. Recently many articles are handling the different physical factors on the peristaltic flow of nanofluids through several conduits [52-62].

2. Aim and Research Significance

The motivation of this research is to study the thermal heating, the gravitational and the slipping effects on the behavior of the peristaltic propulsion of the AuNPs through the blood vessels near to the malignant tumors in the artery. It is also important to select the best shape of the AuNPs amongst three classes of bricks, cylinders, platelets NPs to enhance the natural convection of thermal heating to destroy the neoplasms. The Hamilton-Crosser model is the best and the effective model representing the thermal conductivity of the nanofluid interacted with the shape factor of the nanofluid [32]. The current problem is solved by the perturbation strategy with a small wavenumber perturbation parameter. This is the first try to solve the nanofluids' peristaltic motion using the perturbation method. This study presents a theoretical study of injection of the AuNPs in the blood vessels for cancer therapy application.

3. Problem Formulation

3.1. Geometry Description

The dynamics of the selected model take the effect of peristalsis. The containment involves a non-Newtonian nanofluid with gold Nanoparticles migrated in the blood base fluid through an arterial tube of finite length. The smooth muscles on the tunica media in the middle layer of the blood vessel are the main reason for the peristaltic waves that drive the nanofluid within the artery. Also, the interior surface of the circular tube contains cilia that produce metachronal waves helping the kinetics of the peristaltic pulse in driving the nanofluid. The slipping at these walls and the gravitational effects are also taken into consideration. The undertaken model is exposed to a constant temperature thermal analysis at the external walls. Three types of AuNPs shapes (bricks, cylinders, platelets) are chosen to analyze the ability of the AuNPs shapes on the thermal heating of the malignant tumors, see Figure (1). Hamilton-Crosser model is acceptable to express the effective thermal conductivity of the AuNPs in terms of the

shape factors.

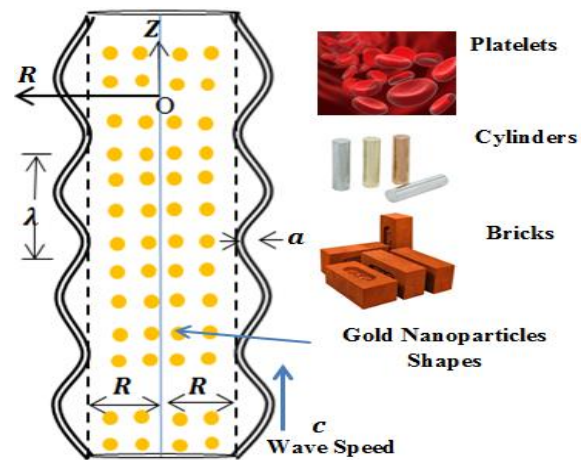


Figure 1- The peristalsis geometry of the dispersed AuNPs in the blood within a tube

The unsteady wavy frame has fixed coordinates (R, Z) and it is converted to a steady wavy frame with coordinates (r, z) moving with the same wave speed c. The z-axis is the streamwise direction of the flow and the R-axis is the radial direction orthogonal to the flow direction. The transformations of the coordinates of the two frames are as follows:

$$r = R, \quad z = Z - ct, \quad u(r, z, t) = U(R, Z, t), \\ w(r, z, t) = W(R, Z, t), \quad p(r, z, t) = P(R, Z, t).$$

3.2. Mathematical Formulation

The differential equations (conservation, momentum, and energy) representing the kinetics of the steady incompressible non-Newtonian nanofluid carrying out the AuNPs injected through the blood base fluid within a tube are expressed as mentioned in [63] as follows.

3.2.1. Governing Equations

• **Continuity**

$$\left(\frac{\partial u}{\partial r} + \frac{u}{r} + \frac{\partial w}{\partial z} \right) = 0, \tag{1}$$

• **r-momentum**

$$\rho_{nf} \left(u \frac{\partial u}{\partial r} + w \frac{\partial u}{\partial z} \right) = - \frac{\partial p}{\partial r} + \\ \mu_{nf} \left(\frac{\partial^2 u}{\partial r^2} + \frac{1}{r} \frac{\partial u}{\partial r} - \frac{u}{r^2} + \frac{\partial^2 u}{\partial z^2} \right) + \rho_{nf} g \alpha (T - T_o), \tag{2}$$

• **z-momentum**

$$\rho_{nf} \left(u \frac{\partial w}{\partial r} + w \frac{\partial w}{\partial z} \right) = - \frac{\partial p}{\partial z} + \\ \mu_{nf} \left(\frac{\partial^2 w}{\partial r^2} + \frac{1}{r} \frac{\partial w}{\partial r} + \frac{\partial^2 w}{\partial z^2} \right), \tag{3}$$

• **Energy**

$$u \frac{\partial T}{\partial r} + w \frac{\partial T}{\partial z} = \alpha_{nf} \left(\frac{\partial^2 T}{\partial r^2} + \frac{1}{r} \frac{\partial T}{\partial r} + \frac{\partial^2 T}{\partial z^2} \right) + Q_o. \tag{4}$$

The height of the flexible tubes takes the form of sinusoidal wave which propagates vertically as follows

$$r = R + \eta(Z, t) = R + a \cos \frac{2\pi}{\lambda}(Z - ct), \quad (5)$$

The nanofluid density, effective dynamic viscosity, and the heat capacitance take the form of [64] as follows:

$$\left. \begin{aligned} \rho_{nf} &= (1 - \phi)\rho_f + \phi\rho_s, \\ \mu_{nf} &= \frac{\mu_f}{(1 - \phi)^{2.5}}, \\ (\rho Cp)_{nf} &= (1 - \phi)(\rho Cp)_f + \phi(\rho Cp)_s. \end{aligned} \right\} \quad (6)$$

The Hamilton-Crosser model expresses the effective thermal conductivity of the nanofluid in terms of the AuNPs shape factor according to [32] as follows:

$$k_{nf} = k_f \left(\frac{k_s + (m + 1)k_f - (m + 1)(k_f - k_s)\phi}{k_s + (m + 1)k_f + (k_f - k_s)\phi} \right), \quad (7)$$

Table (1) gives the three types of the AuNPs and their corresponding values of the shape factor. Table (2) shows the nanofluid physical properties which consists from the base fluid (blood) and the injected NPs (gold) through the blood vessels as [65].

Table 1- The three types of AuNPs and their shape factors

Nanoparticles class	The shape	The shape factor
Bricks		3.7
Cylinders		4.9
Platelets		5.7

Table 2- The nanofluid physical and thermal properties

Thermophysical properties	Blood (base fluid)	Gold (AuNPs)
Cp (J/Kg.oK)	3594	128.8
ρ (Kg/m3)	1063	19320
k(W/m.oK)	0.492	314.4

3.2.2. Boundary Conditions

This section expresses the suitable physical conditions of the undertaken problem which helps a lot in understanding and analyzing the nanofluid behavior according to the slipping velocity and the thermal heating at the walls which will be transferred to the AuNPs to enhance the physical features of the nanofluid to kill the malignancy cells. These conditions are verified at the boundaries at $r = (R + \eta)$ as follows:

The Slipping case is

$$w(r, z, t) = -A \frac{\partial w}{\partial r}, \quad (8)$$

The fully developed case with maximum streamwise velocity at the core of the tube ($r = 0$) is

$$\frac{\partial w(r, z, t)}{\partial r} = 0, \quad (9)$$

The radial velocity at the tube core ($r = 0$) vanishes as

$$u(r, z, t) = 0, \quad (10)$$

The isothermal thermal heating at walls with constant temperature at the external surface is

$$T = T_o, \quad (11)$$

The temperature distribution at the tube centerline ($r = 0$) achieves the case of symmetry as:

$$\frac{\partial T}{\partial r} = 0. \quad (12)$$

3.2.3. Boundary Conditions

The used nondimensional quantities and parameters are introduced as follows:

$$\bar{z} = \frac{z}{\lambda}, \bar{r} = \frac{r}{R}, \bar{\eta} = \frac{\eta}{R}, \bar{u} = \frac{\lambda u}{Rc}, \bar{w} = \frac{w}{c}, \quad (13)$$

$$\bar{t} = \frac{tc}{R}, \bar{p} = \frac{R^2 p}{c \lambda \mu_f}, \bar{\alpha}_{nf} = \frac{\alpha_{nf}}{Rc}, \bar{Q}_o = \frac{Q_o}{Rc},$$

$$\bar{\alpha}_{nf} = \frac{k_{nf}}{\rho_{nf} Cp_{nf}}, \bar{\delta} = \frac{R}{\lambda}, \bar{\epsilon} = \frac{a}{R}, \bar{\beta} = \frac{Q_o R^2}{T_o k_f}, \quad (14)$$

$$Kn = \frac{A}{R}, Gr = \frac{\rho_{nf} g \alpha T_o R^2}{c \mu_f}, Re = \frac{\rho_f c R}{\mu_f}, \theta = \frac{T - T_o}{T_o}. \quad (15)$$

Applying the dimensionless analysis (13-15) on the nanofluid governing and boundary equations (1-5) and (8-12) results in the next system of differential equations after dropping the overbars as follows:

The governing equations are

$$\frac{\partial u}{\partial r} + \frac{u}{r} + \frac{\partial w}{\partial z} = 0, \quad (16)$$

$$\delta Re \frac{\rho_{nf}}{\rho_f} \left(u \frac{\partial w}{\partial r} + w \frac{\partial w}{\partial z} \right) = - \frac{\partial p}{\partial z} + \frac{\mu_{nf}}{\mu_f} \left(\frac{\partial^2 w}{\partial r^2} + \frac{1}{r} \frac{\partial w}{\partial r} + \delta^2 \frac{\partial^2 w}{\partial z^2} \right) + Gr \theta, \quad (17)$$

$$\delta^3 Re \frac{\rho_{nf}}{\rho_f} \left(u \frac{\partial u}{\partial r} + w \frac{\partial u}{\partial z} \right) = - \frac{\partial p}{\partial r} + \frac{\mu_{nf}}{\mu_f} \left[\delta^2 \left(\frac{\partial^2 u}{\partial r^2} + \frac{1}{r} \frac{\partial u}{\partial r} - \frac{u}{r^2} \right) + \delta^4 \frac{\partial^2 u}{\partial z^2} \right], \quad (18)$$

$$\frac{\delta}{\alpha_{nf}} \left(u \frac{\partial \theta}{\partial r} + w \frac{\partial \theta}{\partial z} \right) = \left(\frac{\partial^2 \theta}{\partial r^2} + \frac{1}{r} \frac{\partial \theta}{\partial r} + \delta^2 \frac{\partial^2 \theta}{\partial z^2} \right) + \beta \frac{k_f}{k_{nf}}. \quad (19)$$

The boundary conditions:

At the cylinder walls ($r = h(z) = (1 + \eta) = 1 + \epsilon \cos(2\pi z)$) are

$$w(r, z) = -Kn \frac{\partial w(r, z)}{\partial r}, \quad (20)$$

$$\theta(r, z) = 0, \quad (21)$$

At the cylinder core (r = 0) are

$$\frac{\partial w(r, z)}{\partial r} = 0, \quad (22)$$

$$u(r, z) = 0, \quad (23)$$

$$\frac{\partial \theta(r, z)}{\partial r} = 0, \quad (24)$$

4. Method of Solution

The executed strategy for solving the system of governing equations is the perturbation strategy. It represents a power series expansion for the physical parameters of the nanofluid with a small wave number δ . The pressure gradient is supposed to be constant.

$$w = w_o + \delta w_1 + \delta^2 w_2 + \delta^3 w_3 + \dots, \quad (25)$$

$$u = u_o + \delta u_1 + \delta^2 u_2 + \delta^3 u_3 + \dots, \quad (26)$$

$$\theta = \theta_o + \delta \theta_1 + \delta^2 \theta_2 + \delta^3 \theta_3 + \dots, \quad (27)$$

$$\frac{\partial p}{\partial z} = \left(\frac{\partial p}{\partial z}\right)_o + \delta \left(\frac{\partial p}{\partial z}\right)_1 + \delta^2 \left(\frac{\partial p}{\partial z}\right)_2 + \delta^3 \left(\frac{\partial p}{\partial z}\right)_3 + \dots \quad (28)$$

The steps of the perturbation strategy depend on using the power series of (25-28) in the problem governing equations (16-19) and their boundary conditions (20-24). This procedure results in three systems of equations (zero, first, and second) sets as follows:

The zero set is

$$\frac{\partial u_o}{\partial r} + \frac{u_o}{r} + \frac{\partial w_o}{\partial z} = 0, \quad (29)$$

$$-\left(\frac{\partial p}{\partial z}\right)_o + \frac{\mu_{nf}}{\mu_f} \left(\frac{\partial^2 w_o}{\partial r^2} + \frac{1}{r} \frac{\partial w_o}{\partial r}\right) + Gr \theta_o = 0, \quad (30)$$

$$\frac{\partial^2 \theta_o}{\partial r^2} + \frac{1}{r} \frac{\partial \theta_o}{\partial r} + \beta \frac{k_f}{k_{nf}} = 0. \quad (31)$$

With their boundary conditions

$$w_o(h, z) = -Kn \frac{\partial w_o(h, z)}{\partial r}, \quad (32)$$

$$\frac{\partial w_o(0, z)}{\partial r} = 0, \quad (33)$$

$$\frac{\partial \theta_o(0, z)}{\partial r} = 0, \quad (34)$$

$$\theta_o(h, z) = 0, \quad (35)$$

$$u_o(0, z) = 0, \quad (36)$$

The first set is

$$\frac{\partial u_1}{\partial r} + \frac{u_1}{r} + \frac{\partial w_1}{\partial z} = 0, \quad (37)$$

$$Re \frac{\rho_{nf}}{\rho_f} \left(u_o \frac{\partial w_o}{\partial r} + w_o \frac{\partial w_o}{\partial z}\right) = -\left(\frac{\partial p}{\partial z}\right)_1 +$$

$$\frac{\mu_{nf}}{\mu_f} \left(\frac{\partial^2 w_1}{\partial r^2} + \frac{1}{r} \frac{\partial w_1}{\partial r}\right) + Gr \theta_1, \quad (38)$$

$$\frac{1}{\alpha_{nf}} \left(u_o \frac{\partial \theta_o}{\partial r} + w_o \frac{\partial \theta_o}{\partial z}\right) = \left(\frac{\partial^2 \theta_1}{\partial r^2} + \frac{1}{r} \frac{\partial \theta_1}{\partial r}\right). \quad (39)$$

With their boundary conditions

$$w_1(h, z) = -Kn \frac{\partial w_1(h, z)}{\partial r}, \quad (40)$$

$$\frac{\partial w_1(0, z)}{\partial r} = 0, \quad (41)$$

$$\frac{\partial \theta_1(0, z)}{\partial r} = 0, \quad (42)$$

$$\theta_1(h, z) = 0, \quad (43)$$

$$u_1(0, z) = 0, \quad (44)$$

The second set is

$$\frac{\partial u_2}{\partial r} + \frac{u_2}{r} + \frac{\partial w_2}{\partial z} = 0, \quad (45)$$

$$Re \frac{\rho_{nf}}{\rho_f} \left(u_o \frac{\partial w_1}{\partial r} + u_1 \frac{\partial w_o}{\partial r} + w_o \frac{\partial w_1}{\partial z} + w_1 \frac{\partial w_o}{\partial z}\right) = -\left(\frac{\partial p}{\partial z}\right)_2 + \frac{\mu_{nf}}{\mu_f} \left(\frac{\partial^2 w_2}{\partial r^2} + \frac{1}{r} \frac{\partial w_2}{\partial r} + \frac{\partial^2 w_o}{\partial z^2}\right) + Gr \theta_2, \quad (46)$$

$$\frac{1}{\alpha_{nf}} \left(u_o \frac{\partial \theta_1}{\partial r} + u_1 \frac{\partial \theta_o}{\partial r} + w_o \frac{\partial \theta_1}{\partial z} + w_1 \frac{\partial \theta_o}{\partial z}\right) = \left(\frac{\partial^2 \theta_2}{\partial r^2} + \frac{1}{r} \frac{\partial \theta_2}{\partial r} + \frac{\partial^2 \theta_o}{\partial z^2}\right). \quad (47)$$

With their boundary conditions

$$w_2(h, z) = -Kn \frac{\partial w_2(h, z)}{\partial r}, \quad (48)$$

$$\frac{\partial w_2(0, z)}{\partial r} = 0, \quad (49)$$

$$\frac{\partial \theta_2(0, z)}{\partial r} = 0, \quad (50)$$

$$\theta_2(h, z) = 0, \quad (51)$$

$$u_2(0, z) = 0, \quad (52)$$

Noting that

$$\frac{\partial p(r, z)}{\partial r} = 0 \quad (53)$$

The exact solution for three resulting sets with their boundary conditions is obtained by integrating these differential equations and using their boundary conditions to get their constant.

The solution of the zero-order set is

$$\theta_o = I_1 r^2 + I_2, \quad (54)$$

$$w_o = A_1 r^4 + A_2 r^2 + A_3, \quad (55)$$

$$u_o = L_1 r^5 + L_2 r^3 + L_3 r. \quad (56)$$

The solution of the first order set is

$$\theta_1 = s_{13} r^8 + s_{14} r^6 + s_{15} r^4 + s_{16} r^2 + s_{17}, \quad (57)$$

$$w_1 = g_1 r^{10} + g_2 r^8 + g_3 r^6 + g_4 r^4 + g_5 r^2 + c_2, \quad (58)$$

$$u_1 = F_1 r^{11} + F_2 r^9 + F_3 r^7 + F_4 r^5 + F_5 r^3 + F_6 r. \quad (59)$$

The solution of the second order set is

$$\theta_2 = \frac{B_1}{196} r^{14} + \frac{B_2}{144} r^{12} + \left(\frac{B_3 + B_4}{100}\right) r^{10} + \left(\frac{B_5 + B_6}{64}\right) r^8 + \left(\frac{B_7 + B_8}{64}\right) r^6 + \frac{B_9}{16} r^4 + \frac{B_{10}}{4} r^2 + c_3, \quad (60)$$

$$w_2 = e_1 r^{16} + e_2 r^{14} + (e_3 + e_4) r^{12} + (e_5 + e_6) r^{10} + (e_7 + e_8) r^8 + (e_9 + e_{10}) r^6 + e_{11} r^4 + e_{12} r^2 + c_4, \quad (61)$$

$$u_2 = D_1 r^{17} + D_2 r^{15} + D_3 r^{13} + D_4 r^{11} + D_5 r^9 + D_6 r^7 + D_7 r^5 + D_8 r^3 + D_9 r. \quad (62)$$

The streamlines can be obtained by integrating the next relation.

$$w = -\frac{1}{r} \frac{\partial \psi(r, z)}{\partial r} \quad (63)$$

Also, the streamwise velocity profiles and the temperature distribution are found according to the relations (25) and (27). Noting that, the coefficients and the constants are expressed in the appendix section.

5. Results and Discussion

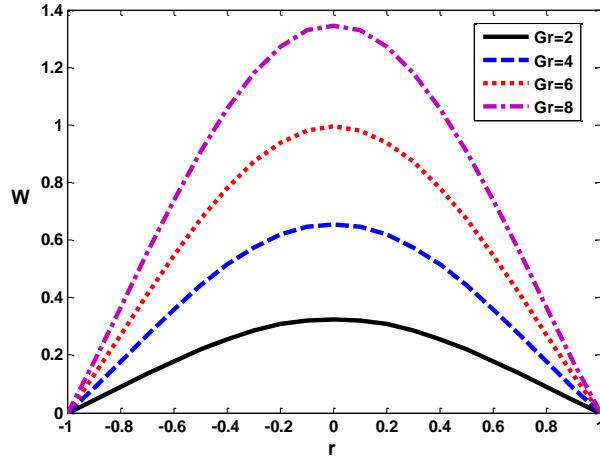
The essential objective of this part is showing and discussing the behavior of the blood flow after injection AuNPs through it in the tube. The deduced expressions for the streamwise velocity, the temperature distributions, and the streamlines are graphically presented and discussed according to the emerging thermophysical properties of the prorogating nanofluid with the aid of MATLAB software. This include the influence of NPs concentrations (ϕ), the shape factors (m), the slipping Knudsen number (Kn), the gravitational Grashof number (Gr), the thermal heat source (β), the perturbation wave number parameter (δ), the peristaltic amplitude ratio (ϵ), the constant pressure gradient ($\frac{dp}{dz}$), and the streamwise location (z) which indicates the local wave shape (tube, expansion, contraction). The pressure gradient is supposed to be constant. The streamwise velocity profiles are plotted in Figures (2–10) with low Reynolds number and small wave number under the impact of the pervious thermophysical properties by making a graphical comparison to show the difference between the two cases of non-slipping and slipping conditions. The data used to indicate the graphs of Figures (2–10) are tabulated in Table (3) for the two cases of conditions; non-slipping condition (Kn = 0) and slipping condition (Kn = 0.1). The platelets shape is chosen to represent the AuNPs surface geometry. The constant negative pressure gradient ($\frac{dp}{dz} < 0$) is favorable, as it means the flow occurs in the streamwise direction

without any reversal flow. The back flow and the separation phenomenon occur according to the positive pressure gradient ($\frac{dp}{dz} > 0$).

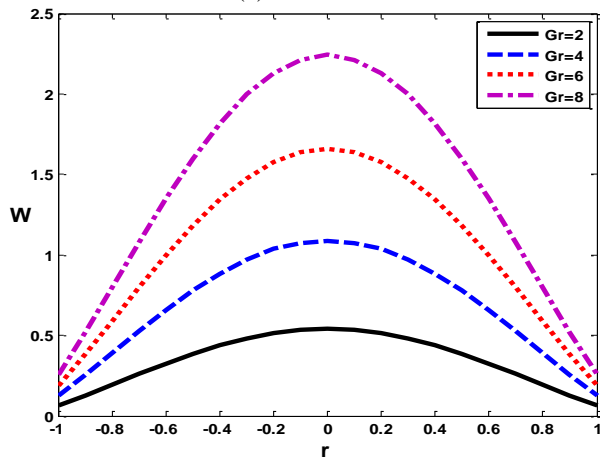
Figure (2) indicates the enhancement in the streamwise velocity as a result of increasing the gravitational Grashof number. This effect appears in both cases of non-slipping (Kn = 0) and slipping (Kn = 0.1). The velocity profiles are higher in case of slipping and the slipping effect is very obvious at the walls as it raises the relative velocity at the boundaries. Figure (3) takes a look on the shape and the direction of the flow of the nanofluid according to the pressure gradient sign for both cases of slipping and non-slipping. It is also observed that the favorable pressure gradient is the negative as the fully developed flow exists and no separation occurs while the adverse pressure gradient takes the positive sign and causes the reversal flow. The zero-pressure gradient isn't preferable as the velocity profiles are small and seem to be constant but it still better than positive pressure gradient. The slipping effect increases the velocity near the walls and makes the trend of the velocity profiles higher than these exist in the non-slipping case. It is noticed in Figure (4) that the raise in the heat source intensity causes a growth in the net axial velocity profiles. The high concentration of the volume fraction for the AuNPs resists the flow motion and reduces the streamwise velocity as plotted in Figure (5). The shape and the surface geometry of the AuNPs has a great impact on the streamwise velocity of the nanofluid. Figure (6) shows that, the platelets shape of AuNPs has the lowest velocity profile while the velocity profiles are greater in case of the shape of bricks. Thus, to enhance the streamwise velocity, the selected shape of the AuNPS is the bricks shape. The sharpness of the peristalsis which is responsible for the motion of the nanofluid is specified according to the amplitude ratio. It is observed in Figures (7–8) that the boosting in the streamwise velocity profiles occurs because of the increase in the wave number and the wave amplitude ratio, respectively. The streamwise location (z) controls the values of the axial velocity. The velocity profile is high at the location where the expansion occurs ($r = 1 + \epsilon$) and the axial velocity falls down at the location of uniform tube ($r = 1$), whilst at the location of contraction ($r = 1 - \epsilon$) takes the lowest axial velocity profile; see Figure (9).

From the pictorial view of the net axial velocity profiles in case of the slipping conditions, the net axial velocity takes higher magnitudes than the non-slipping ones at the core of the tube and at the boundaries as shown for (Kn = 0.1) in Figures (2–9). This is confirmed by Figure (10), which shows the effect of slipping and non-slipping conditions on the behavior

of the nanofluid, it is noticed that the increase in the slipping flow (Kn) is boosting the streamwise velocity.

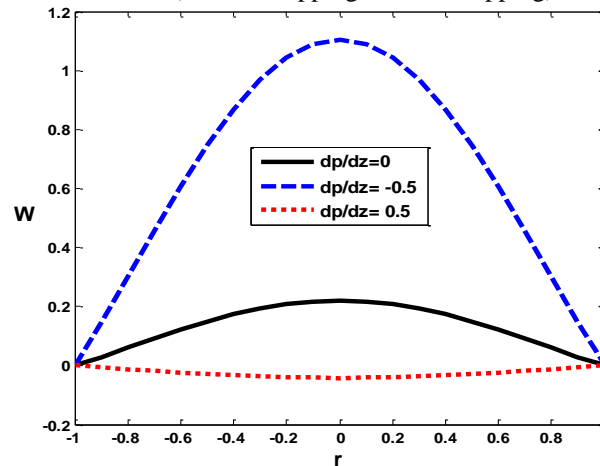


(a) $Kn = 0$

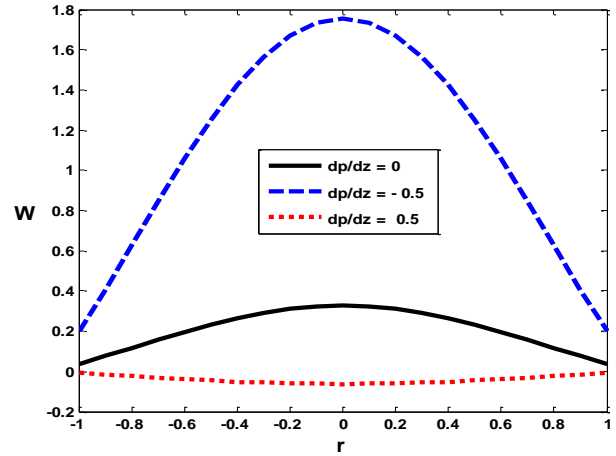


(b) $Kn = 0.1$

Figure 2- Effect of the gravitational Grashof number on the streamwise velocity profiles for the blood flow of nanofluid (cases of slipping and non-slipping)

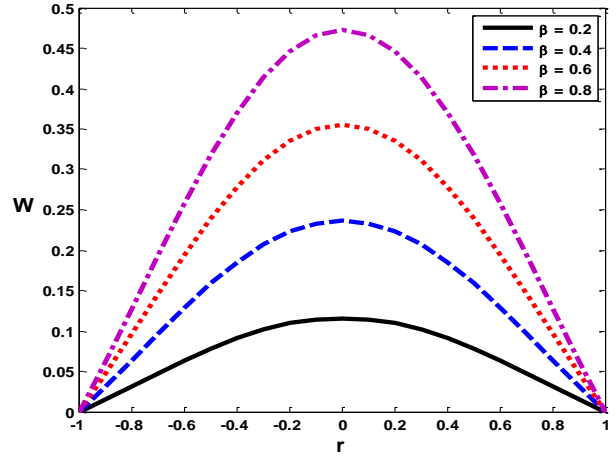


(a) $Kn = 0$

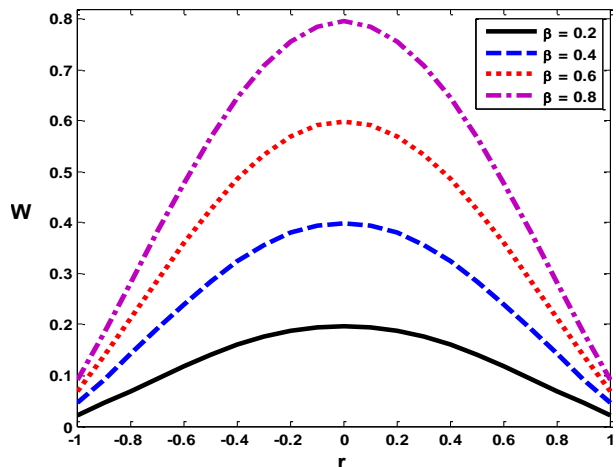


(b) $Kn = 0.1$

Figure 3- Effect of the pressure gradient on the streamwise velocity profiles for the blood flow of nanofluid (cases of slipping and non-slipping)

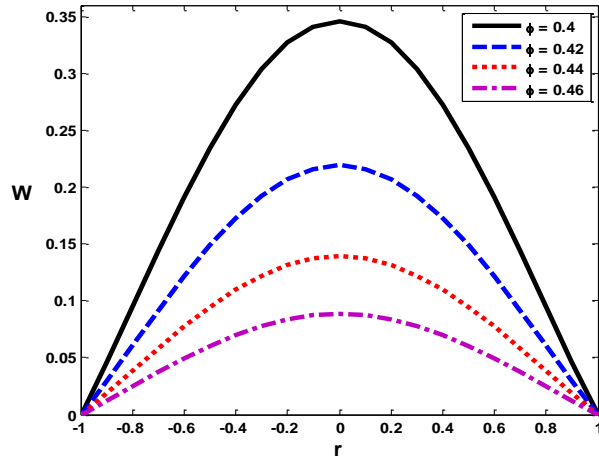


(a) $Kn = 0$

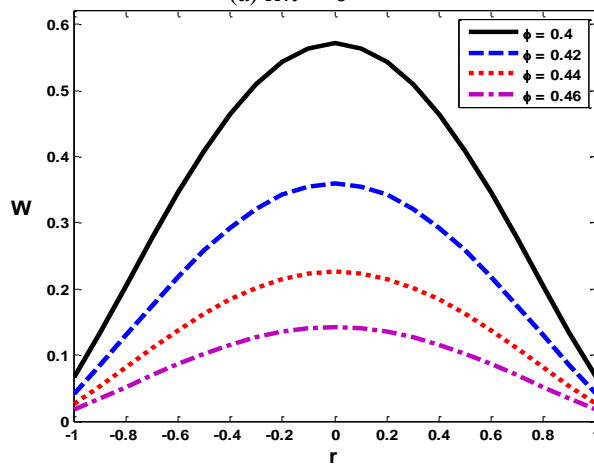


(b) $Kn = 0.1$

Figure 4- Effect of the thermal heat source on the streamwise velocity profiles for the blood flow of nanofluid (cases of slipping and non-slipping)

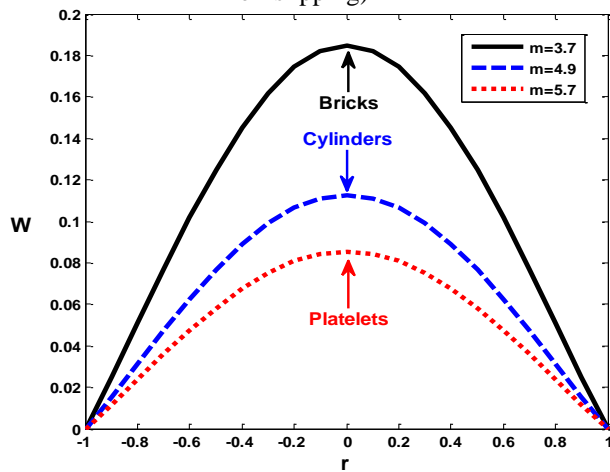


(a) $Kn = 0$

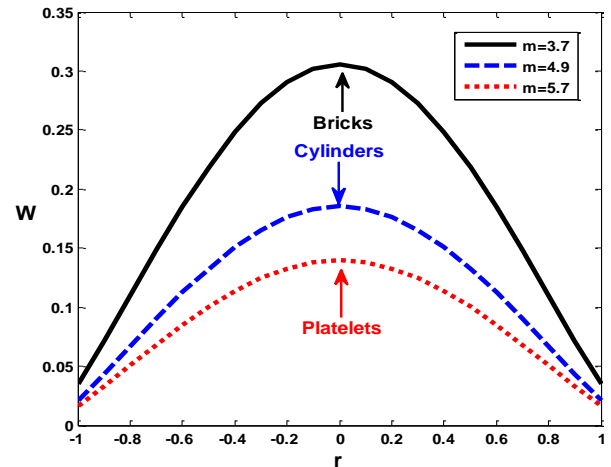


(b) $Kn = 0.1$

Figure 5- Effect of the influence of NPs concentrations on the streamwise velocity profiles for the blood flow of nanofluid (cases of slipping and non-slipping)

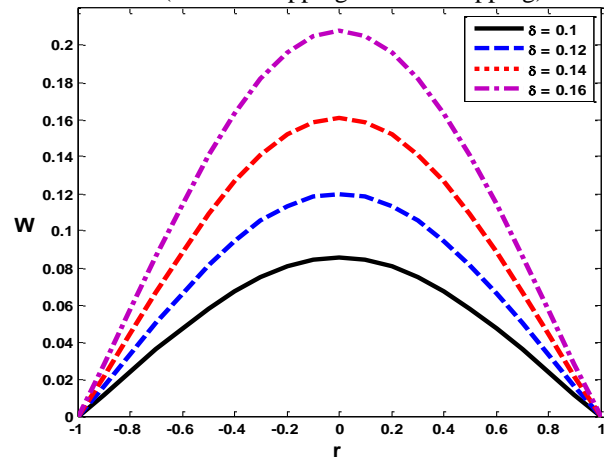


(a) $Kn = 0$

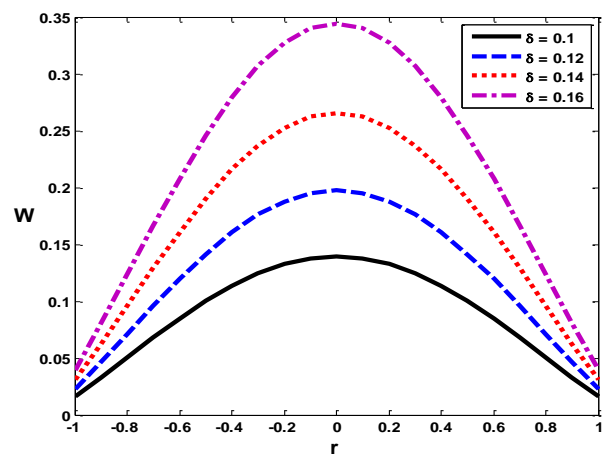


(b) $Kn = 0.1$

Figure 6- Effect of the shape factors on the streamwise velocity profiles for the blood flow of nanofluid (cases of slipping and non-slipping)

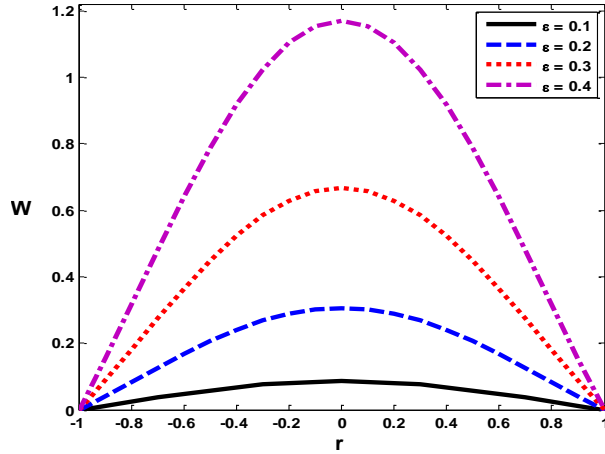


(a) $Kn = 0$

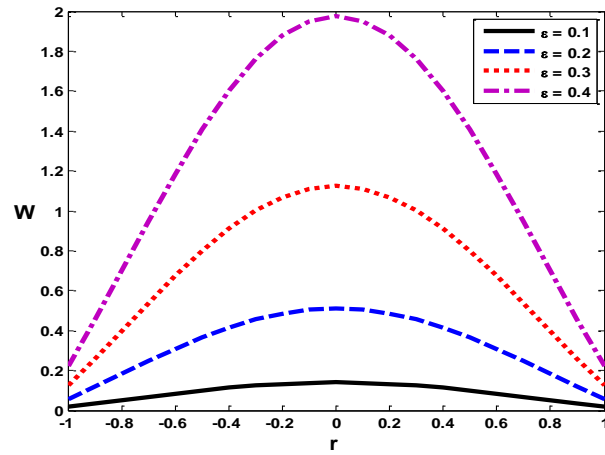


(b) $Kn = 0.1$

Figure 7- Effect of the wave number parameter on the streamwise velocity profiles for the blood flow of nanofluid (cases of slipping and non-slipping)

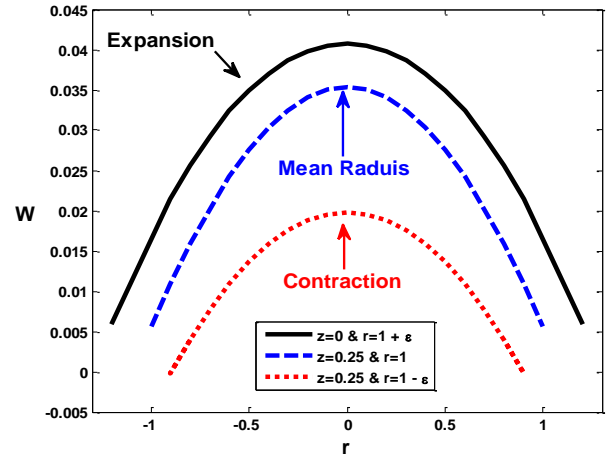


(a) $Kn = 0$



(b) $Kn = 0.1$

Figure 8- Effect of the amplitude ratio on the streamwise velocity profiles for the blood flow of nanofluid (cases of slipping and non-slipping)



(b) $Kn = 0.1$

Figure 9- Effect of the streamwise location on the streamwise velocity profiles for the blood flow of nanofluid (cases of slipping and non-slipping)

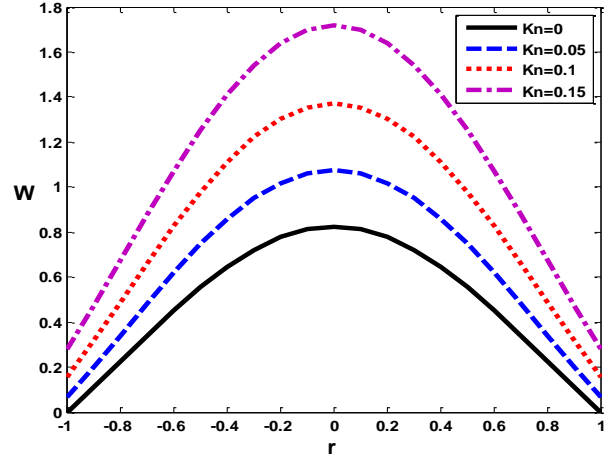
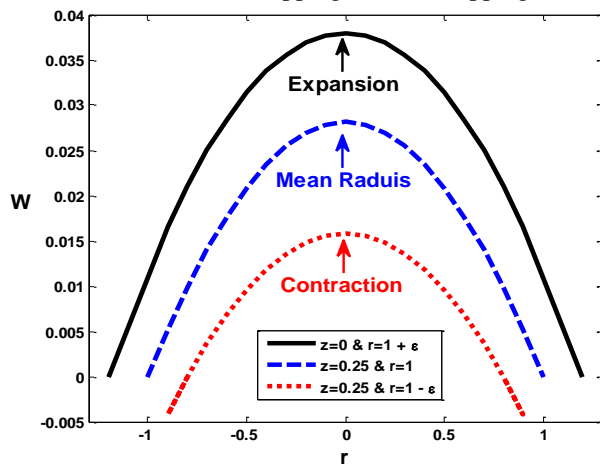


Figure 10- Effect of the slipping parameter (Knudsen number) on the streamwise velocity profiles for the blood flow of nanofluid.



(a) $Kn = 0$

Table 3- Thermophysical Parameters Corresponding to Figures (2–9)

Thermophysical parameters Figures	Gr	$\frac{dp}{dz}$	β	ϕ	m	δ	ε	z	Re
Figure 2	2	-0.5	0.2	0.7	5.7	0.1	0.1	0.25	0.5
	4								
	6								
	8								
Figure 3	8	0	5	0.7	5.7	0.01	0.1	0.25	0.2
		-0.5							
		0.5							
Figure 4	0.8	-0.5	0.2	0.7	5.7	0.1	0.1	0.25	0.2
			0.4						
			0.6						
			0.8						
Figure 5	0.2	-0.2	0.2	0.4	5.7	0.01	0.1	0.25	0.5
				0.42					
				0.44					
				0.46					
Figure 6	0.2	-0.5	0.5	0.7	3.7	0.1	0.1	0.25	0.5
					4.9				
					5.7				
Figure 7	0.2	-0.5	0.5	0.7	5.7	0.1	0.1	0.25	0.5
						0.12			
						0.14			
						0.16			
Figure 8	0.2	-0.5	0.5	0.7	5.7	0.1	0.1	0.25	0.5
							0.2		
							0.3		
							0.4		
Figure 9	0.8	-2	0.8	0.7	5.7	0.01	0.2	0	0.2
								0.25	
								0.5	
Figure 10	0.2	-0.5	5	0.7	5.7	0.1	0.1	0.25	5

The thermal heating effect appears by plotting the temperature distribution profiles for the two cases of conditions; non-slipping condition ($Kn = 0$) and slipping condition ($Kn = 0.1$) as shown in Figure (11–17). These profiles are expressing the convective heating and the ability of the AuNPs to absorb and transfer the heat to the malignant cells in the blood. The related data expressing the different values of the thermophysical properties corresponding to Figure (11–16) are tabulated in Table (4) for the two cases of conditions; non-slipping condition ($Kn = 0$) and for the slipping condition ($Kn = 0.1$). From the graphs of

the temperature distributions, the nanofluid temperature inside the core of the tube is the greatest and the temperature decreases along the tube up to the boundaries. Figures (11–13) show that the nanofluid temperature distribution is growing by raising the heat source intensity, the Grashof number and the peristalsis amplitude ratio. In contrast, the crowd on AuNPs concentrations reduces the temperature distributions as noticed in Figure (14).

The shape of nanoparticles and its surface area has a vital role in the heat absorption and the heat transfer. The bricks shape has the highest surface area, then the

cylindrical shape and the platelets shape has the lowest surface area. As a result, the bricks shape has the largest temperature distributions, the cylindrical shape reduces the temperature distributions but still larger than the temperature in case of the platelets shape. Then the bricks shape is recommended as a best AuNPs shape for conveying the heat and giving highest temperature, see Figure (15). The z location affects the temperature distribution in Figure (16) as the temperature falls down by changing the location from the expansion position ($r = 1 + \epsilon$), the tube ($r = 1$), and the contraction position ($r = 1 - \epsilon$), respectively. From the photographic view of the temperature distribution profiles in case of the slipping condition ($Kn = 0.1$) as shown in Figures (11–16), it is observed that, the magnitude and the trend of the temperature distribution profiles are high compared with the non-slipping condition ($Kn = 0$). This is confirmed by Figure (17), which shows that the effect of slipping and non-slipping conditions on the temperature distribution profiles, it is noticed that the temperature distribution of the nanofluid enhancing by augmenting in the slipping flux (Knudsen number Kn) enhances the temperature distribution of the nanofluid.

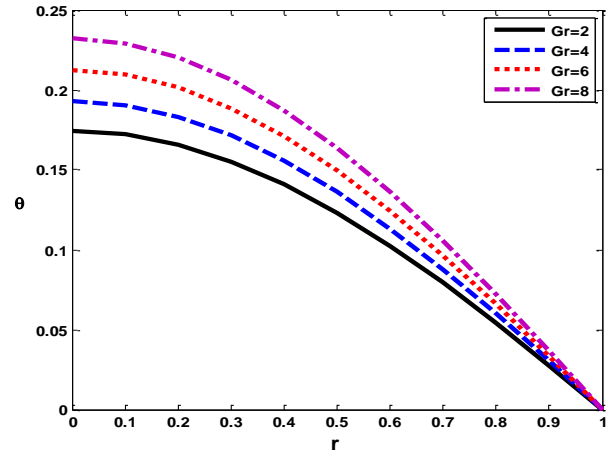
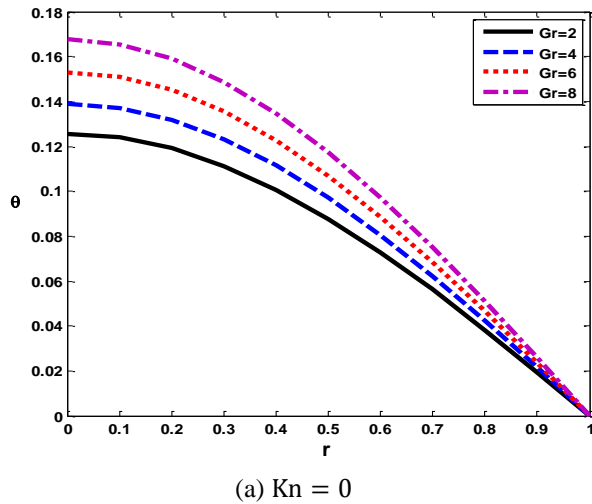


Figure 11- Effect of the gravitational Grashof number on the temperature distribution profiles for the blood flow of nanofluid (cases of slipping and non-slipping)

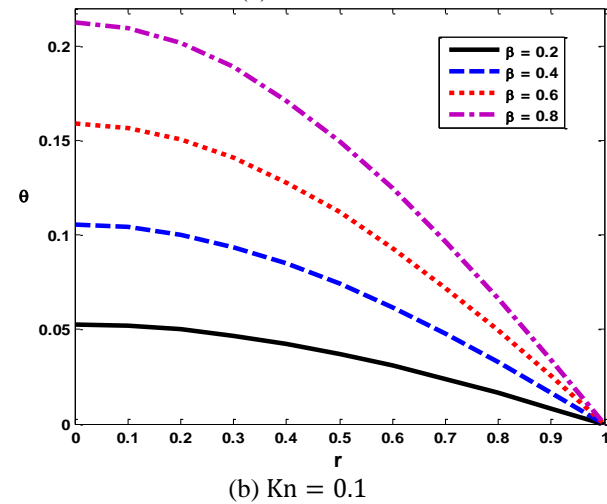
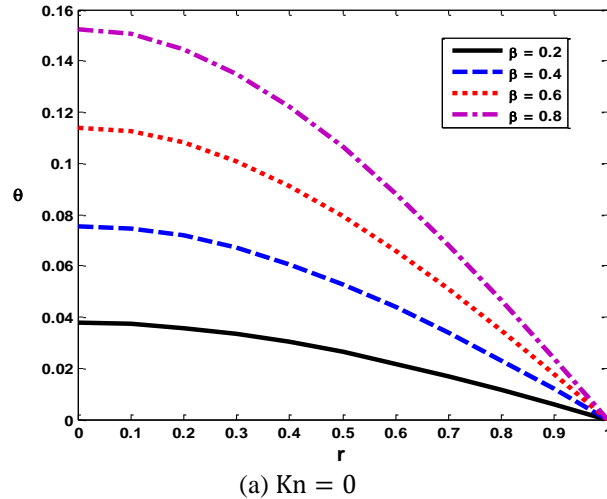
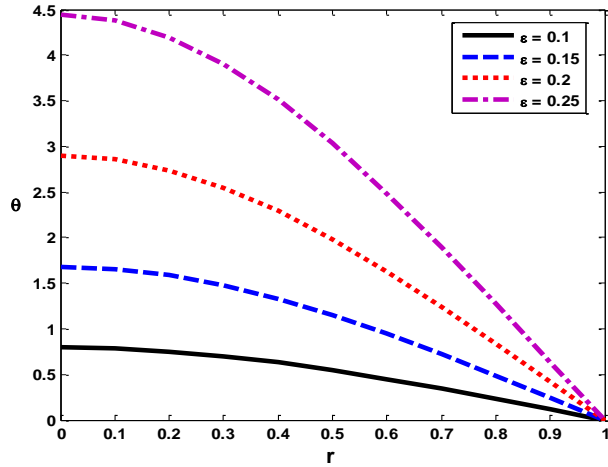
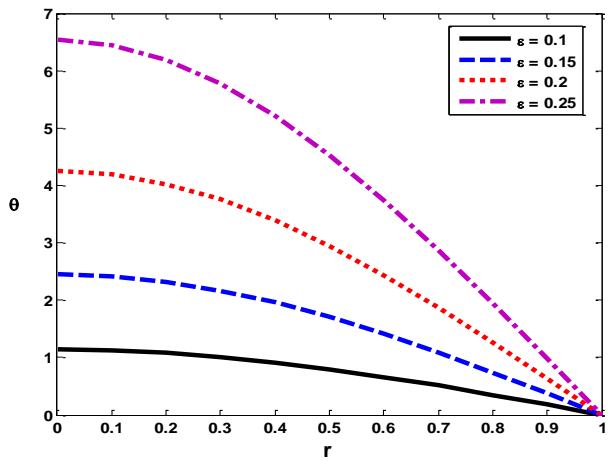


Figure 12- Effect of the thermal heat source on the temperature distribution profiles for the blood flow of nanofluid (cases of slipping and non-slipping)

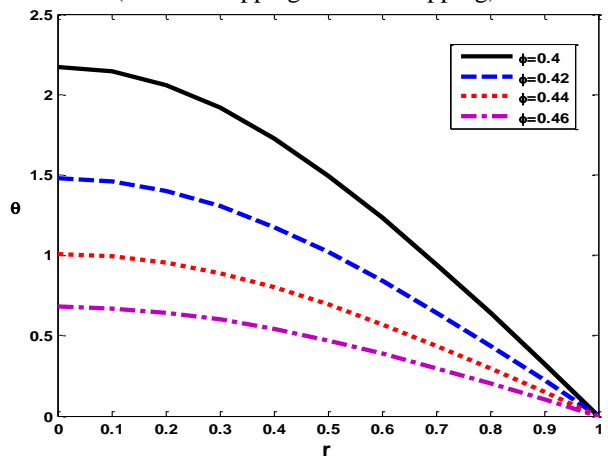


(a) $Kn = 0$

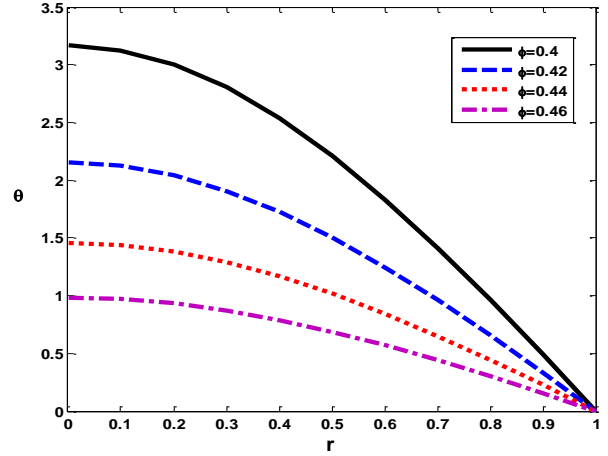


(b) $Kn = 0.1$

Figure 13- Effect of the amplitude ratio on the temperature distribution profiles for the blood flow of nanofluid (cases of slipping and non-slipping)

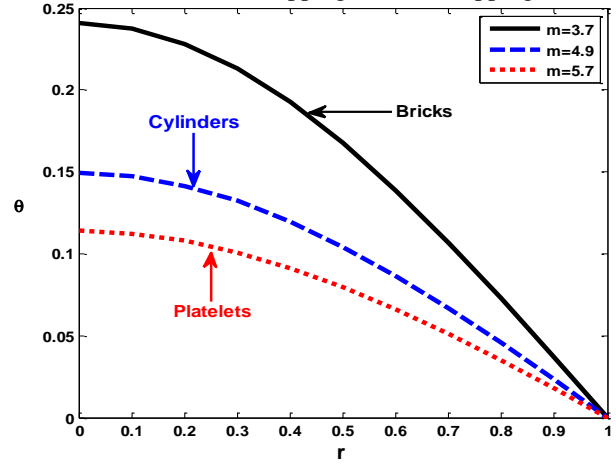


(a) $Kn = 0$

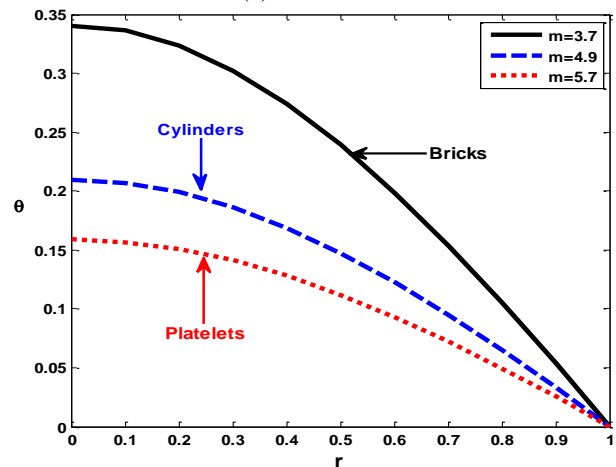


(b) $Kn = 0.1$

Figure 14- Effect of the NPs concentrations on the temperature distribution profiles for the blood flow of nanofluid (cases of slipping and non-slipping)



(a) $Kn = 0$

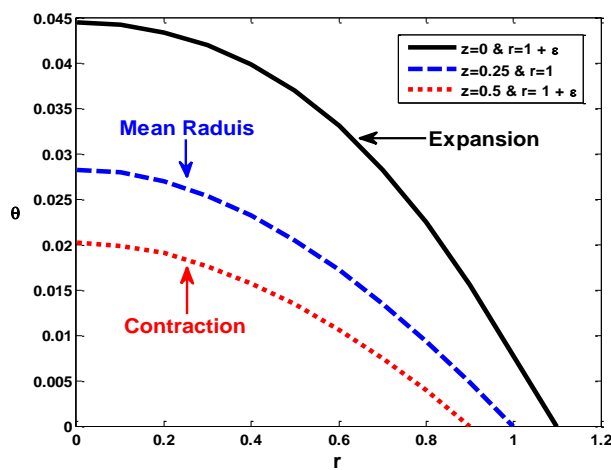


(b) $Kn = 0.1$

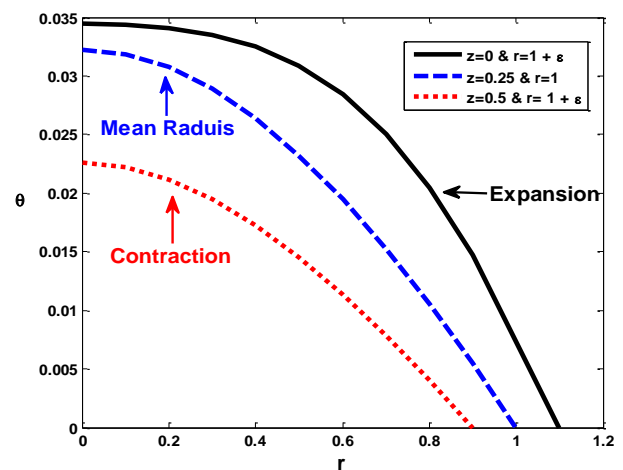
Figure 15- Effect of the shape factors on the temperature distribution profiles for the blood flow of nanofluid (cases of slipping and non-slipping)

Table 4- Thermophysical Parameters Corresponding to Figures (11–16)

Thermophysical parameters Figures	Gr	$\frac{dp}{dz}$	β	ε	ϕ	m	δ	z	Re
Figure 11	2	-0.2	0.6	0.1	0.7	5.7	0.01	0.25	0.2
	4								
	6								
	8								
Figure 12	0.8	-0.2	0.2	0.1	0.7	5.7	0.01	0.25	0.2
			0.4						
			0.6						
			0.8						
Figure 13	0.2	-0.5	0.8	0.1	0.7	5.7	0.01	0.25	0.2
				0.15					
				0.2					
				0.25					
Figure 14	0.2	-0.5	0.2	0.1	0.4	5.7	0.001	0.25	0.2
					0.42				
					0.44				
					0.46				
Figure 15	0.2	-0.2	0.6	0.1	0.7	3.7	0.01	0.25	0.2
						4.9			
						5.7			
Figure 16	2	-0.5	2	0.1	0.7	5.7	0.001	0	0.2
								0.25	
								0.5	
Figure 17	0.2	-0.2	0.6	0.1	0.7	5.7	0.01	0.25	2



(a) $Kn = 0$



(b) $Kn = 0.1$

Figure 16- Effect of the streamwise location on the temperature distribution profiles for the blood flow of nanofluid (cases of slipping and non-slipping)

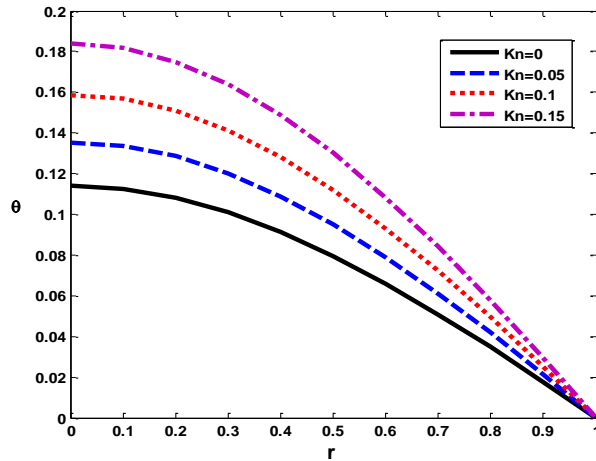
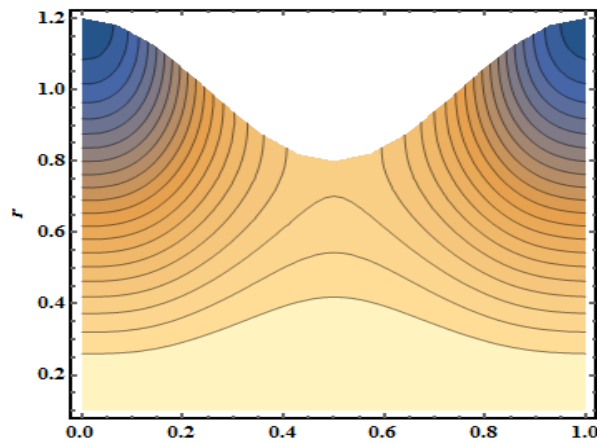
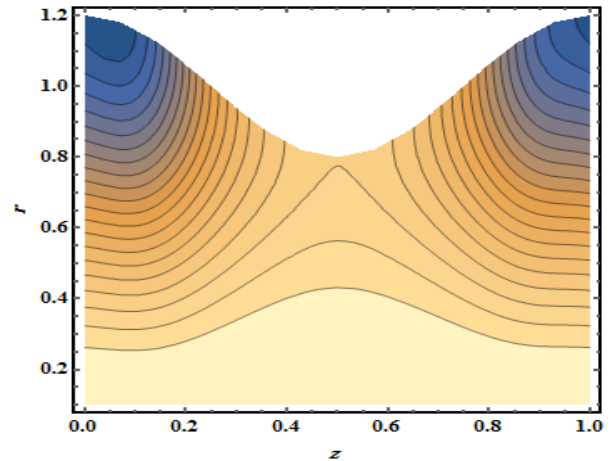


Figure 17- Effect of the slipping parameter (Knudsen number) on the temperature distribution profiles for the blood flow of nanofluid.

The streamlines curves of the blood flow of nanofluid along the tube radius are illustrated in Figures (18–22) and the related data for the thermophysical parameters are tabulated in Table (5). The smooth eddies are occurring near the boundaries, but the contours are uniform near the core of the tube. The contours of the blood flow of nanofluid streamlines are closing each other in case of non-slipping flow and these contours are spaced enough according to the slipping conditions as shown in Figure (22). The increase in the gravitational Grashof number (Gr) and heat source intensity (β) causes the shape of contours of the streamlines more uniform as illustrated in Figures (18–19). Figure (20) shows that the raise of the AuNPs concentration (ϕ) make the contours closes to each other and eddies are increased. The different shapes of the AuNPs have approximately the same effect on the shape of the enclosed streamlines contours as shown in Figure (21).

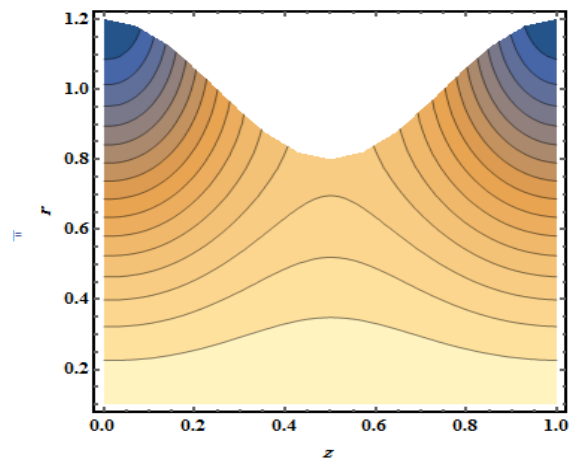


(a) $Gr = 2$

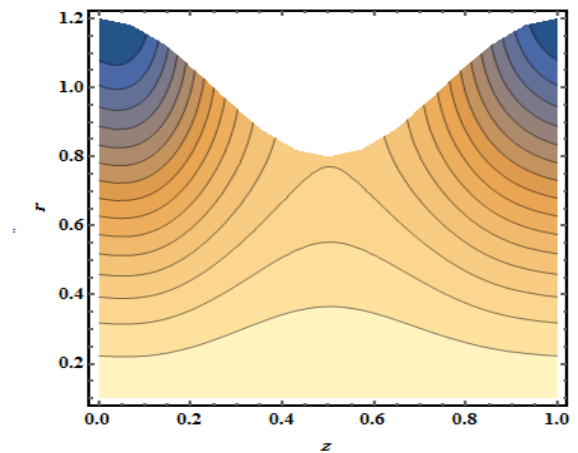


(b) $Gr = 8$

Figure 18- Effect of the gravitational Grashof number on the Stramlines contours along the tube axis

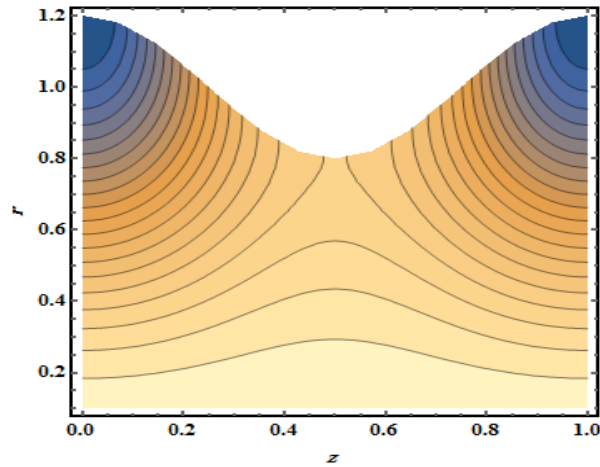


(a) $\beta = 2$

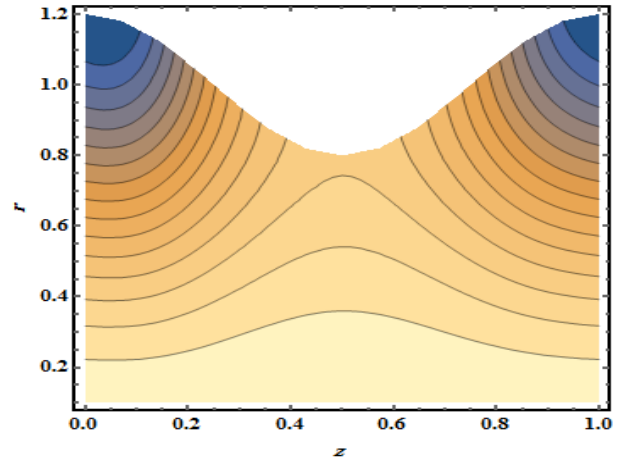


(b) $\beta = 8$

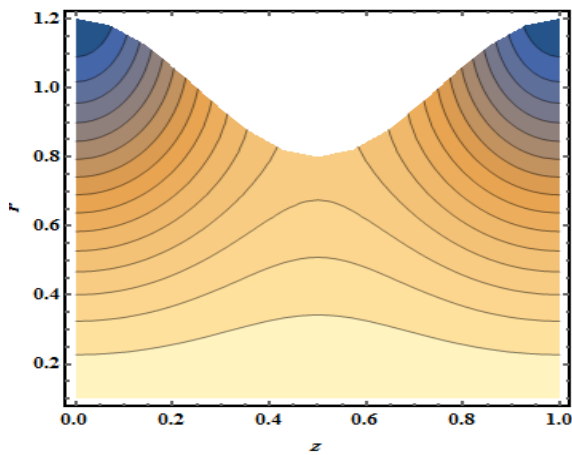
Figure 19- Effect of the thermal heat source on the Stramlines contours along the tube axis



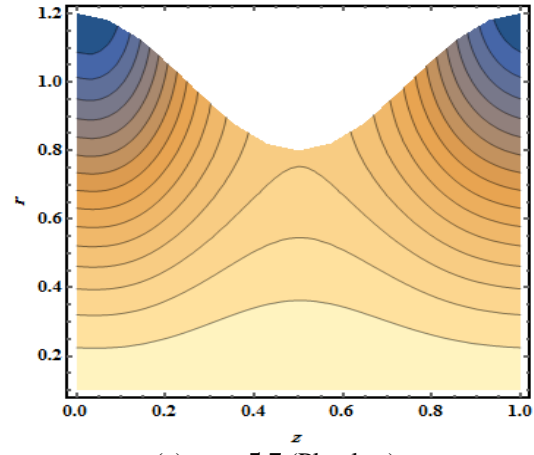
(a) $\phi = 0.1$



(b) $m = 4.9$ (Cylinders)



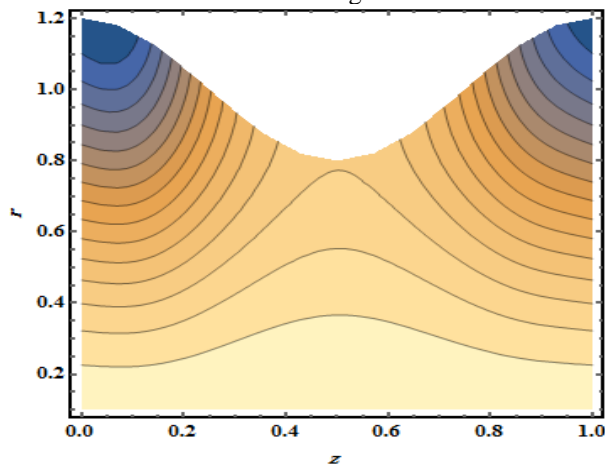
(b) $\phi = 0.5$



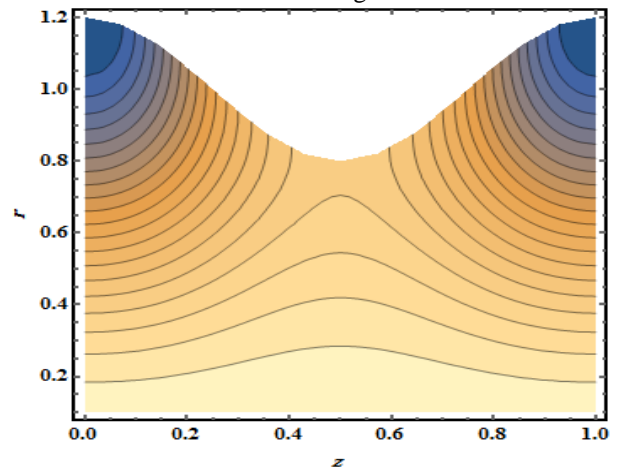
(c) $m = 5.7$ (Platelets)

Figure 20- Effect of the NPs concentrations on the Stramlines contours along the tube axis

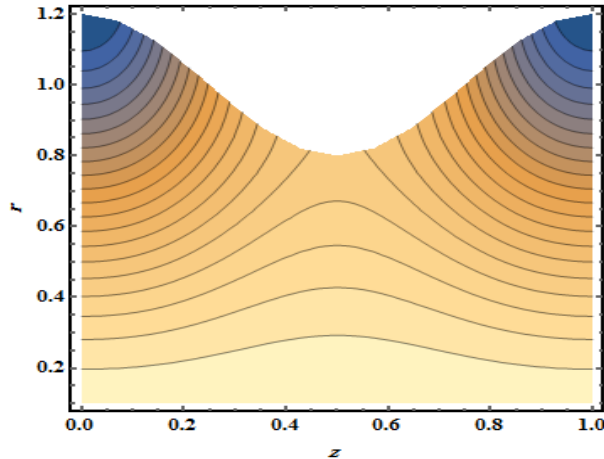
Figure 21- Effect of the shape factors on the Stramlines contours along the tube axis



(a) $m = 3.7$ (Bricks)



(a) $Kn = 0$



(b) $Kn = 0.1$

Figure 22- Effect of the slipping parameter (Knudsen number) on the Stramlines contours along the tube axis

Accuracy Check

This study represents the initial attempt at addressing peristaltic motion of nanofluids within a tube using the perturbation technique. The accuracy of the solution is validated as the derived differential equations for velocity and temperature agree with those obtained by

Akbar and Butt [51] in the absence of slipping conditions. It is worth noting that the graphical results of this study for velocity distribution under no-slip conditions approaches with the findings of Akbar and Butt [51] in the absence of magnetic field effects as shown in Figure (23).

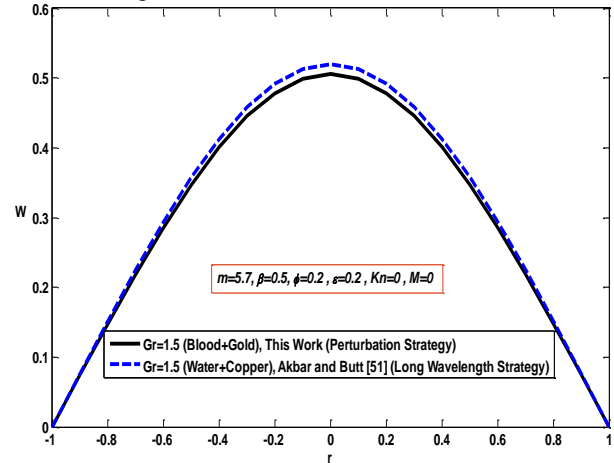


Figure 23- Velocity distribution under the effect of Grashof number for accuracy check and validation

Table 5- Thermophysical Parameters Corresponding to Figures (18–22)

<i>Thermophysical parameters</i>	Gr	$\frac{dp}{dz}$	β	ϕ	m	δ	ϵ	Re	Kn
<i>Figures</i>									
<i>Figure 18</i>	2	-0.5	0.2	0.7	5.7	0.01	0.2	0.5	0.1
	8								
<i>Figure 19</i>	2	-0.5	2	0.7	5.7	0.001	0.2	0.5	0.1
			8						
<i>Figure 20</i>	2	-0.5	0.2	0.1	5.7	0.01	0.2	0.5	0.1
				0.5					
<i>Figure 21</i>	2	-0.5	6	0.7	3.7	0.001	0.2	0.5	0.1
					4.9				
					5.7				
<i>Figure 22</i>	0.8	-0.5	0.1	0.7	5.7	0.01	0.2	0.5	0
									0.1

6. Conclusions

This research is handling the action of several thermophysical properties of the nanofluid such as the

heat source intensity, the gravitational effect, the slipping at walls, the nanoparticles shape factor, the peristalsis amplitude ratio, and the solid nanoparticles

concentration on the behavior of the nanofluid flow through a vertical tube. The dynamics of the blood flow of nanofluid flow occur according to the peristaltic action. The nanofluid consists of the blood as a basis fluid and the gold as injection nanoparticles into the bloodstream. The Hamilton-Crosser model is selected to express the performance and the effectiveness of the thermic conductivity of the AuNPs in terms of the shape factor. The streamwise velocity AuNPs through the blood in presence of thermal heating is a good model representing the photothermal therapy to eliminate the malignance cells in the blood vessels. The concluding remarks of the results of the problem are as follows:

1. The intensity of the heat source and the gravitational Grashof number are enhancing the streamwise velocity and the temperature distributions of the nanoparticles.
2. The net axial velocity and the temperature distribution profiles in case of slipping flow are high unlike the non-slipping case.
3. The bricks AuNps are enhancing the thermal heating and for boosting the streamwise velocity likewise platelets AuNPs.
4. The increase in the AuNPs concentration reduces the net axial velocity and decreases the temperature distribution.

profiles, the temperature distribution, and the streamlines contours are plotted under the influence of the pervious properties. Three shapes of AuNPs (bricks, cylinders, and platelets) are chosen to represent the best surface geometry to measure their ability for the heat absorption and transfer the heat. The perturbation strategy is used for solving the problem governing equations with long wavelength and low Reynolds number. The injection of the

5. The adverse pressure gradient ($\frac{dp}{dx} > 0$) resists the flow and the reversal flow exists likewise the negative pressure gradient. The contours of the streamlines are enclosed for the non-slipping condition unlike the slipping case and the eddies are existing near the boundaries and the countours are uniform near the core of the tube.
6. The contours of the streamlines are enclosed for the non-slipping condition unlike the slipping case and the eddies are existing near the boundaries and the countours are uniform near the core of the tube.

Nomenclature

z	.The streamwise flow direction
r	The radial direction orthogonal to flow direction.
R	.The tube mean radius
η	.The vertical wall displacement
c	.The peristaltic wave speed
p	.The nanofluid pressure
T	.The nanofluid Temperature
T_o	.The reference temperature
ρ_{nf}	.The nanofluid density
μ_{nf}	The nanofluid effective dynamic viscosity.
α_{nf}	The nanofluid effective thermal diffusivity.
ρ_s	The density of the gold nanoparticles.
ρ_f	The density of the base fluid.
μ_f	The base fluid effective dynamic viscosity.
k_s	The gold nanoparticles thermal conductivity.
k_{nf}	The nanofluid effective thermal conductivity
ϕ	.The volume fraction coefficient
m	The gold nanoparticles shape factor.
$(\rho Cp)_s$	The gold nanoparticles heat capacitance.

$(\rho Cp)_f$	The base fluid heat capacitance.
$(\rho Cp)_{nf}$.The nanofluid heat capacitance
$C_{p_{nf}}$	The nanofluid specific heat at constant pressure.
α	.The volume expansion coefficient
Q_o	.The Heat Source
t	.The time
g	.The gravity
a	.The wave amplitude
λ	.The wavelength
Gr	.Grashof number
β	.Heat source coefficient
ε	.The amplitude ratio
δ	.The sinusoidal wave number
θ	.The dimensionless temperature
Re	.Reynolds number
A	The mean free path of the base fluid.
Kn	.The slipping Knudsen number

Appendix

$h = 1 + \varepsilon \cos(2\pi z), K_o = \frac{\mu_f}{\mu_{nf}} = \frac{1}{(1-\phi)^{2.5}}, K_1 = \frac{Gr \beta k_f}{k_{nf}}, K_2 = \frac{\beta k_f}{k_{nf}},$
$K_3 = \frac{Re \rho_{nf}}{\rho_f}, K_4 = K_3 K_o^3 \left(\frac{dp}{dz}\right)_o^2, K_5 = K_1 K_3 K_o^3 \left(\frac{dp}{dz}\right)_o, K_6 = K_o^3 K_1^2 K_3,$
$K_7 = \frac{K_o K_2}{\alpha_{nf}} \left(\frac{dp}{dz}\right)_o, K_8 = \frac{K_o K_1 K_2}{\alpha_{nf}}, I_1 = \frac{-K_2}{4}, I_2 = \frac{K_2 h^2}{4}, A_1 = \frac{K_o K_1}{64},$
$A_2 = \frac{K_o}{64} \left(\frac{dp}{dz}\right)_o - \frac{K_o K_1 h^2}{16}, A_3 = K_o \left(\frac{dp}{dz}\right)_o \left[\frac{-Kn h}{2} - \frac{h^2}{4}\right] + K_o K_1 \left[\frac{3h^4}{64} + \frac{Kn h^3}{16}\right], L_1 = \frac{-K_o K_1}{384},$
$L_2 = -\left[\frac{K_o}{16} \left(\frac{dp}{dz}\right)_o + \frac{K_o K_1 h h'}{32}\right], L_3 = K_o \left(\frac{dp}{dz}\right)_o \left[\frac{h h'}{8} + \frac{Kn h'}{4}\right] + K_o K_1 \left[\frac{-3Kn h^2 h'}{32} + \frac{3h^3 h'}{32}\right],$
$S_1 = \frac{-3h h'}{16} + \frac{Kn h'}{8}, S_2 = \frac{-1}{32}, S_3 = \frac{-3h^2 h'}{4} + \frac{Kn^2 h h'}{4} + h^3 h', S_4 = \frac{-3h h'}{128} + \frac{Kn h'}{128} + \frac{h^2}{128},$
$S_5 = \frac{7h^3 h'}{64} + \frac{Kn h h^2}{16}, S_6 = \frac{-1}{192}, S_7 = \frac{-9h^5 h'}{64} + \frac{3h^4 h'}{32} - \frac{23Kn h^4 h'}{128} - \frac{(-3Kn + Kn^2) h^3 h'}{32},$
$S_8 = \frac{h^2}{3072}, S_9 = \frac{-1}{6144}, S_{10} = \frac{h^3 h'}{1024} - \frac{3Kn h h^2}{1024}, S_{11} = \frac{3h^4 h'}{256} - \frac{3h^5 h'}{512} + \frac{Kn h h^4}{256},$
$S_{12} = \frac{9h^7 h'}{1024} + \frac{5Kn h^6 h'}{512} + \frac{3Kn^2 h h^5}{256}, S_{13} = \frac{K_8}{49152}, S_{14} = \frac{K_7}{1152} - \frac{K_8 h h'}{4608},$
$S_{15} = K_8 \left(\frac{h^3 h'}{1024} + \frac{3Kn h^2 h'}{1280}\right) + \frac{K_7 h h'}{256}, S_{16} = K_8 \left(\frac{3h^5 h'}{512} + \frac{Kn h^4 h'}{128}\right) + K_7 \left(\frac{-Kn h^2 h'}{16} - \frac{h^3 h'}{32}\right),$
$S_{17} = K_8 \left(\frac{-61h^7 h'}{9216} - \frac{13Kn h^6 h'}{1280} - \frac{h^8}{49152}\right) + K_7 \left(\frac{Kn h^4 h'}{16} + \frac{7h^5 h'}{256} - \frac{h^6}{1152}\right),$
$m_1 = S_9 K_6 - K_o Gr S_{13}, m_2 = S_6 K_5 + S_8 K_6 - K_o Gr S_{14},$
$m_3 = S_2 K_4 + S_4 K_5 + S_{10} K_6 - K_o Gr S_{15}, m_4 = S_1 K_4 + S_5 K_5 + S_{11} K_6 - K_o Gr S_{16},$
$m_5 = S_3 K_4 + S_7 K_5 + S_{12} K_6 - K_o Gr S_{17}, g_1 = \frac{m_1}{100}, g_2 = \frac{m_2}{64}, g_3 = \frac{m_3}{36}, g_4 = \frac{m_4}{16},$
$g_5 = \frac{m_5}{4} + \frac{K_o}{4} \left(\frac{dp}{dz}\right)_1, F_1 = \frac{-m'_1}{1200}, F_2 = \frac{-m'_2}{640}, F_3 = \frac{-m'_3}{288}, F_4 = \frac{-m'_4}{96}, F_5 = \frac{-m'_5}{16},$
$F_6 = \frac{-c'_2}{2}, B_1 = \frac{1}{\alpha_{nf}} [8L_1 S_{13} + 2I_1 F_1 + A_1 S'_{13} + g_1 I'_1], B_4 = \frac{1}{\alpha_{nf}} [2I_1 F_3 + g_3 I'_1],$
$B_2 = \frac{1}{\alpha_{nf}} [6L_1 S_{14} + 8L_2 S_{13} + 2I_1 F_2 + A_1 S'_{14} + A_2 S'_{13} + g_2 I'_1 + g_1 I'_2],$
$B_3 = \frac{1}{\alpha_{nf}} [4L_1 S_{15} + 6L_2 S_{14} + 8L_3 S_{13} + A_1 S'_{15} + A_2 S'_{14} + A_3 S'_{13} + g_2 I'_2],$
$B_5 = \frac{1}{\alpha_{nf}} [2L_1 S_{16} + 4L_2 S_{15} + 6L_3 S_{14} + A_1 S'_{16} + A_2 S'_{15} + A_3 S'_{14}], B_6 = \frac{1}{\alpha_{nf}} [2I_1 F_4 + g_4 I'_1 + g_3 I'_2],$
$B_7 = \frac{1}{\alpha_{nf}} [2L_2 S_{16} + 4L_3 S_{15} + 2I_1 F_5 + A_1 S'_{17} + A_2 S'_{16} + A_3 S'_{15} + g_5 I'_1], B_8 = \frac{g_4 I'_2}{\alpha_{nf}},$
$B_9 = \frac{1}{\alpha_{nf}} [2L_3 S_{16} + 2I_1 F_1 + A_2 S'_{17} + A_3 S'_{16} + c_2 I'_1 + g_5 I'_2], B_{10} = \frac{1}{\alpha_{nf}} [A_3 S'_{17} + c_2 I'_2] + I''_2,$

$c_2 = -m_1 \left[\frac{Knh^9}{10} + \frac{h^{10}}{100} \right] - m_2 \left[\frac{Knh^7}{8} + \frac{h^8}{64} \right] - m_3 \left[\frac{Knh^5}{6} + \frac{h^6}{36} \right] - m_4 \left[\frac{Knh^3}{4} + \frac{h^4}{16} \right] - m_5 \left[\frac{Knh}{2} + \frac{h^2}{4} \right] - K_o \left(\frac{dp}{dz} \right)_1 \left[\frac{Knh}{2} + \frac{h^2}{4} \right]$
$c_3 = - \left[\frac{B_1}{196} h^{14} + \frac{B_2}{144} h^{12} + \left(\frac{B_3 + B_4}{100} \right) h^{10} + \left(\frac{B_5 + B_6}{64} \right) h^8 + \left(\frac{B_7 + B_8}{64} \right) h^6 + \frac{B_9}{16} h^4 + \frac{B_{10}}{4} h^2 \right],$
$c_4 = -a_1 \left[\frac{Knh^{15}}{16} + \frac{h^{16}}{256} \right] - a_2 \left[\frac{Knh^{13}}{14} + \frac{h^{14}}{196} \right] - (a_3 + a_4) \left[\frac{Knh^{11}}{12} + \frac{h^{12}}{144} \right] -$
$(a_5 + a_6) \left[\frac{Knh^9}{10} + \frac{h^{10}}{100} \right] - (a_7 + a_8) \left[\frac{Knh^7}{8} + \frac{h^8}{64} \right] - (a_9 + a_{10}) \left[\frac{Knh^5}{6} + \frac{h^6}{36} \right] - a_{11} \left[\frac{Knh^3}{4} + \frac{h^4}{16} \right] - a_{12} \left[\frac{Knh}{2} + \frac{h^2}{4} \right],$
$a_1 = \left[K_o K_3 (10 g_1 L_1 + 4 A_1 F_1 + A_1 g'_1 + A'_1 g_1) - \frac{K_o Gr B_1}{196} \right],$
$a_2 = \left[K_o K_3 (8 g_2 L_1 + 10 g_1 L_2 + 4 A_1 F_2 + 2 A_2 F_1 + A_1 g'_2 + A_2 g'_1 + A'_1 g_2 + A'_2 g_1) - \frac{K_o Gr B_2}{144} \right],$
$a_3 = \left[K_o K_3 (8 g_2 L_2 + 10 g_1 L_3 + 2 A_2 F_2 + A_2 g'_2 + A_3 g'_1 + A'_2 g_2 + A'_3 g_1) - \frac{K_o Gr B_3}{100} \right],$
$a_4 = \left[K_o K_3 (5 g_3 L_1 + 4 A_1 F_3 + A_1 g'_3 + A'_1 g_3) - \frac{K_o Gr B_4}{81} \right],$
$a_5 = \left[K_o K_3 (8 g_2 L_3 + A_3 g'_2 + A'_3 g_2) - \frac{K_o Gr B_5}{64} \right],$
$a_6 = \left[K_o K_3 (3 g_4 L_1 + 5 g_3 L_2 + 4 A_1 F_4 + 2 A_2 F_3 + A_1 g'_4 + A_2 g'_3 + A'_1 g_4 + A'_3 g_2) - \frac{K_o Gr B_6}{49} \right],$
$a_7 = \left[K_o K_3 (2 g_5 L_1 + 4 A_1 F_5 + A_1 g'_5 + A'_1 g_5) - \frac{K_o Gr B_7}{36} \right],$
$a_8 = \left[K_o K_3 (3 g_4 L_2 + 5 g_3 L_3 + 2 A_2 F_4 + A_2 g'_4 + A_3 g'_3 + A'_2 g_4 + A'_3 g_3) - \frac{K_o Gr B_8}{25} \right],$
$a_9 = \left[K_o K_3 (2 g_5 L_2 + 4 A_1 F_6 + 2 A_2 F_5 + A_1 c'_2 + A_2 g'_5 + A'_1 c_2 + A'_2 g_5) - \frac{K_o Gr B_9}{16} - A''_1 \right],$
$a_{10} = \left[K_o K_3 (3 g_4 L_3 + A_3 g'_4 + A'_3 g_4) \right],$
$a_{11} = \left[K_o K_3 (2 g_5 L_3 + 2 A_2 F_6 + A_2 c'_2 + A_3 g'_5 + A'_2 c_2 + A_3 g_5) - \frac{K_o Gr B_{10}}{4} - A''_2 \right],$
$a_{12} = \left[K_o K_3 (A_2 c'_2 + A_3 c'_2) - K_o Gr c_3 - A''_3 + \left(\frac{dp}{dz} \right)_2 \right], e_1 = \frac{a_1}{256}, e_2 = \frac{a_2}{196}, e_3 = \frac{a_3}{144},$
$e_4 = \frac{a_4}{144}, e_5 = \frac{a_5}{100}, e_6 = \frac{a_6}{100}, e_7 = \frac{a_7}{64}, e_8 = \frac{a_8}{64}, e_9 = \frac{a_9}{36}, e_{10} = \frac{a_{10}}{36}, e_{11} = \frac{a_{11}}{16}, e_{12} = \frac{a_{12}}{4},$
$D_1 = -\frac{e'_1}{18}, D_2 = -\frac{e'_2}{16}, D_3 = -\left(\frac{e'_3 + e'_4}{14} \right), D_4 = -\left(\frac{e'_5 + e'_6}{12} \right), D_5 = -\left(\frac{e'_7 + e'_8}{10} \right),$
$D_6 = -\left(\frac{e'_9 + e'_{10}}{8} \right), D_9 = -\frac{c'_4}{2} \text{ and } D_8 = -\frac{e'_{12}}{4}, D_7 = -\frac{e'_{11}}{6},$

6. References

- [1] W. Cai, T. Gao, H. Hong, and J. Sun, "Applications of gold nanoparticles in cancer nanotechnology," *Nanotechnology, science and applications*, vol. 1, p. 17, 2008.
- [2] F. Razmi, R. K. Moghaddam, and A. Rowhanimanesh, "Control of cancer growth using single input autonomous fuzzy Nano-particles," *Journal of Fuzzy Set Valued Analysis*, vol. 1, no. 2015, pp. 86-96, 2015.
- [3] P. K. Jain, W. Qian, and M. A. El-Sayed, "Ultrafast cooling of photoexcited electrons in gold nanoparticle– thiolated DNA conjugates involves the dissociation of the gold– thiol bond," *Journal of the American Chemical Society*, vol. 128, no. 7, pp. 2426-2433, 2006.
- [4] N. R. Jana, L. Gearheart, and C. J. Murphy, "Wet chemical synthesis of high aspect ratio cylindrical gold nanorods," *The Journal of Physical Chemistry B*, vol. 105, no. 19, pp. 4065-4067, 2001.
- [5] N. R. Jana, L. Gearheart, S. O. Obare, and C. J. Murphy, "Anisotropic chemical reactivity of gold spheroids and nanorods," *Langmuir*, vol. 18, no. 3, pp. 922-927, 2002.
- [6] A. Jemal et al., "Cancer statistics, 2008," *CA: a cancer journal for clinicians*, vol. 58, no. 2, pp. 71-96, 2008.
- [7] A. Shrivastava and H. Garg, "Application of Nanotechnology and Biocomputation for Treatment of Cancer: A Review," *The Pharma Innovation*, vol. 2, no. 6, 2013.
- [8] P. K. Jain, K. S. Lee, I. H. El-Sayed, and M. A. El-Sayed, "Calculated absorption and scattering properties of gold nanoparticles of different size, shape, and composition: applications in biological imaging and biomedicine," *The journal of physical chemistry B*, vol. 110, no. 14, pp. 7238-7248, 2006.
- [9] I. Eldesoky, "Influence of slip condition on peristaltic transport of a compressible Maxwell fluid through porous medium in a tube," *International Journal of Applied Mathematics and Mechanics*, vol. 8, no. 2, pp. 99-117, 2012.
- [10] I. Eldesoky, R. Abumandour, M. Kamel, and E. Abdelwahab, "The combined influences of heat transfer, compliant wall properties and slip conditions on the peristaltic flow through tube," *SN Applied Sciences*, vol. 1, no. 8, p. 897, 2019.
- [11] I. M. Eldesoky, R. M. Abumandour, and E. T. Abdelwahab, "Analysis for various effects of relaxation time and wall properties on compressible Maxwellian peristaltic slip flow," *Zeitschrift für Naturforschung A*, vol. 74, no. 4, pp. 317-331, 2019.
- [12] M. H. Kamel, I. M. Eldesoky, B. M. Maher, and R. M. Abumandour, "Slip effects on peristaltic transport of a particle-fluid suspension in a planar channel," *Applied bionics and biomechanics*, vol. 2015, 2015.
- [13] L. Srivastava and V. Srivastava, "On two-phase model of pulsatile blood flow with entrance effects," *Biorheology*, vol. 20, no. 6, pp. 761-777, 1983.
- [14] L. Srivastava and V. Srivastava, "Peristaltic transport of blood: Casson model—II," *Journal of Biomechanics*, vol. 17, no. 11, pp. 821-829, 1984.
- [15] L. Srivastava and V. Srivastava, "Interaction of peristaltic flow with pulsatile flow in a circular cylindrical tube," *Journal of biomechanics*, vol. 18, no. 4, pp. 247-253, 1985.
- [16] L. Srivastava and V. Srivastava, "Peristaltic transport of a particle-fluid suspension," *Journal of biomechanical engineering*, vol. 111, no. 2, pp. 157-165, 1989.
- [17] V. Srivastava and M. Saxena, "A two-fluid model of non-Newtonian blood flow induced by peristaltic waves," *Rheologica Acta*, vol. 34, no. 4, pp. 406-414, 1995.
- [18] V. Srivastava and L. Srivastava, "Effects of Poiseuille flow on peristaltic transport of a particulate suspension," *Zeitschrift für angewandte Mathematik und Physik ZAMP*, vol. 46, no. 5, pp. 655-679, 1995.
- [19] F. Yin and Y. C. Fung, "Peristaltic waves in circular cylindrical tubes," *Journal of Applied Mechanics*, vol. 36, no. 3, pp. 579-587, 1969.
- [20] I. Eldesoky, S. I. Abdelsalam, W. A. El-Askary, and M. Ahmed, "The integrated thermal effect in conjunction with slip conditions on peristaltically induced particle-fluid transport in a catheterized pipe," *Journal of Porous Media*, vol. 23, no. 7, 2020.
- [21] M. Jaffrin and A. Shapiro, "Peristaltic pumping," *Annual Review of Fluid Mechanics*, vol. 3, no. 1, pp. 13-37, 1971.
- [22] T. W. Latham, "Fluid motions in a peristaltic pump," *Massachusetts Institute of Technology*, 1966.
- [23] A. H. Shapiro, "Pumping and retrograde diffusion in peristaltic waves," in *Proceedings of the workshop in ureteral reflux in children*, Washington, DC, 1967, pp. 109-126.
- [24] A. H. Shapiro, M. Y. Jaffrin, and S. L. Weinberg, "Peristaltic pumping with long wavelengths at low Reynolds number," *Journal of fluid mechanics*, vol. 37, no. 4, pp. 799-825, 1969.
- [25] A. Aarts and G. Ooms, "Net flow of compressible viscous liquids induced by travelling waves in porous media," *Journal of engineering mathematics*, vol. 34, no. 4, pp. 435-450, 1998.
- [26] R. M. Abumandour, I. M. Eldesoky, and E. T. Abdelwahab, "On the Performance of Peristaltic Pumping for the MHD Slip Flow under the Variation of Elastic Walls Features," *ERJ. Engineering Research Journal*, vol. 43, no. 3, pp. 231-244, 2020.

- [27] T. Anwar, M. Tahir, P. Kumam, S. Ahmed, and P. Thounthong, "Magnetohydrodynamic mixed convective peristaltic slip transport of carbon nanotubes dispersed in water through an inclined channel with Joule heating," *Heat Transfer*.
- [28] I. Eldesoky, S. Abdelsalam, R. Abumandour, M. Kamel, and K. Vafai, "Interaction between compressibility and particulate suspension on peristaltically driven flow in planar channel," *Applied Mathematics and Mechanics*, vol. 38, no. 1, pp. 137-154, 2017.
- [29] E. El-Shehawy, N. El-Dabe, and I. El-Desoky, "Slip effects on the peristaltic flow of a non-Newtonian Maxwellian fluid," *Acta Mechanica*, vol. 186, no. 1-4, pp. 141-159, 2006.
- [30] J. Fang, "On the peristaltic transport in small-Knudsen-number flow," *Meccanica*, vol. 35, no. 1, pp. 69-74, 2000.
- [31] S. U. Choi and J. A. Eastman, "Enhancing thermal conductivity of fluids with nanoparticles," Argonne National Lab., IL (United States)1995.
- [32] P. M. Kumar, J. Kumar, R. Tamilarasan, S. Sendhilnathan, and S. Suresh, "Review on nanofluids theoretical thermal conductivity models," *Engineering Journal*, vol. 19, no. 1, pp. 67-83, 2015.
- [33] S. Wang and G. Lu, "Applications of gold nanoparticles in cancer imaging and treatment," *Noble and Precious Metals—Properties, Nanoscale Effects and Applications*; Seehra, MS, Bristow, AD, Eds, pp. 291-309, 2018.
- [34] X. Huang and M. A. El-Sayed, "Gold nanoparticles: Optical properties and implementations in cancer diagnosis and photothermal therapy," *Journal of advanced research*, vol. 1, no. 1, pp. 13-28, 2010.
- [35] N. S. Akbar, A. B. Huda, M. B. Habib, and D. Tripathi, "Nanoparticles shape effects on peristaltic transport of nanofluids in presence of magnetohydrodynamics," *Microsystem Technologies*, vol. 25, no. 1, pp. 283-294, 2019.
- [36] E. C. Dreaden, M. A. Mackey, X. Huang, B. Kang, and M. A. El-Sayed, "Beating cancer in multiple ways using nanogold," *Chemical Society Reviews*, vol. 40, no. 7, pp. 3391-3404, 2011.
- [37] E. C. Dreaden, L. A. Austin, M. A. Mackey, and M. A. El-Sayed, "Size matters: gold nanoparticles in targeted cancer drug delivery," *Therapeutic delivery*, vol. 3, no. 4, pp. 457-478, 2012.
- [38] S. I. Abdelsalam and M. Bhatti, "New insight into AuNP applications in tumour treatment and cosmetics through wavy annuli at the nanoscale," *Scientific reports*, vol. 9, no. 1, pp. 1-14, 2019.
- [39] M. Hatami, J. Hatami, and D. D. Ganji, "Computer simulation of MHD blood conveying gold nanoparticles as a third grade non-Newtonian nanofluid in a hollow porous vessel," *Computer methods and programs in biomedicine*, vol. 113, no. 2, pp. 632-641, 2014.
- [40] K. S. Mekheimer, W. Hasona, R. Abo-Elkhair, and A. Zaher, "Peristaltic blood flow with gold nanoparticles as a third grade nanofluid in catheter: Application of cancer therapy," *Physics Letters A*, vol. 382, no. 2-3, pp. 85-93, 2018.
- [41] A. Hamzehnezhad, M. Fakour, D. Ganji, and A. Rahbari, "Heat transfer and fluid flow of blood flow containing nanoparticles through porous blood vessels with magnetic field," *Math. Biosci.*, vol. 283, pp. 38-47, 2017.
- [42] K. S. Mekheimer, T. Elnaqeeb, M. El Kot, and F. Alghamdi, "Simultaneous effect of magnetic field and metallic nanoparticles on a micropolar fluid through an overlapping stenotic artery: blood flow model," *Physics Essays*, vol. 29, no. 2, pp. 272-283, 2016.
- [43] M. Sheikholeslami and M. Shamlooei, "Magnetic source influence on nanofluid flow in porous medium considering shape factor effect," *Physics Letters A*, vol. 381, no. 36, pp. 3071-3078, 2017.
- [44] M. Sheikholeslami and H. B. Rokni, "Simulation of nanofluid heat transfer in presence of magnetic field: a review," *International Journal of Heat and Mass Transfer*, vol. 115, pp. 1203-1233, 2017.
- [45] R. Ellahi, S. Rahman, and S. Nadeem, "Blood flow of Jeffrey fluid in a catherized tapered artery with the suspension of nanoparticles," *Physics Letters A*, vol. 378, no. 40, pp. 2973-2980, 2014.
- [46] N. S. Akbar, "Peristaltic flow of Cu-water nanofluid in a tube," *Journal of Computational and Theoretical Nanoscience*, vol. 11, no. 6, pp. 1411-1416, 2014.
- [47] H. Sadaf and S. I. Abdelsalam, "Adverse effects of a hybrid nanofluid in a wavy non-uniform annulus with convective boundary conditions," *RSC Advances*, vol. 10, no. 26, pp. 15035-15043, 2020.
- [48] M. M. Bhatti, M. Marin, A. Zeeshan, R. Ellahi, and S. I. Abdelsalam, "Swimming of Motile Gyrotactic Microorganisms and Nanoparticles in Blood Flow Through Anisotropically Tapered Arteries," *Frontiers in Physics*, vol. 8, p. 95, 2020.
- [49] S. Abdelsalam and M. Bhatti, "Anomalous reactivity of thermo-bioconvective nanofluid towards oxytactic microorganisms," *Appl. Math. Mech.*, 2020.
- [50] S. I. Abdelsalam and M. M. Bhatti, "The impact of impinging TiO₂ nanoparticles in Prandtl nanofluid along with endoscopic and variable magnetic field effects on peristaltic blood flow," *Multidiscipline Modeling in Materials and Structures*, 2018.
- [51] N. S. Akbar and A. W. Butt, "Ferromagnetic effects for peristaltic flow of Cu–water nanofluid for

- different shapes of nanosize particles," *Applied Nanoscience*, vol. 6, pp. 379-385, 2016.
- [52] P. Devaki, B. Venkateswarlu, S. Srinivas, and S. Sreenadh, "MHD Peristaltic flow of a nanofluid in a constricted artery for different shapes of nanosized particles," *Nonlinear Engineering*, vol. 9, no. 1, pp. 51-59, 2020.
- [53] N. S. Akbar, D. Tripathi, and O. A. Bég, "Modeling nanoparticle geometry effects on peristaltic pumping of medical magnetohydrodynamic nanofluids with heat transfer," *Journal of Mechanics in Medicine and Biology*, vol. 16, no. 06, p. 1650088, 2016.
- [54] N. S. Akbar, A. B. Huda, and D. Tripathi, "Thermally developing MHD peristaltic transport of nanofluids with velocity and thermal slip effects," *The European Physical Journal Plus*, vol. 131, no. 9, pp. 1-18, 2016.
- [55] S. Sheriff, H. Sadaf, N. S. Akbar, and N. Mir, "Heat and peristaltic propagation of water based nanoparticles with variable fluid features," *Physica Scripta*, vol. 94, no. 12, p. 125704, 2019.
- [56] Q. Afzal and S. Akram, "Impact of double-diffusivity convection in nanofluids and induced magnetic field on peristaltic pumping of a Carreau fluid in a tapered channel with different waveforms," *Journal of Thermal Analysis and Calorimetry*, vol. 143, pp. 2291-2312, 2021.
- [57] S. I. Abdelsalam, A. Magesh, P. Tamizharasi, and A. Zaher, "Versatile response of a Sutterby nanofluid under activation energy: hyperthermia therapy," *International Journal of Numerical Methods for Heat & Fluid Flow*, 2023.
- [58] S. I. Abdelsalam, A. M. Alsharif, Y. Abd Elmaboud, and A. Abdellateef, "Assorted kerosene-based nanofluid across a dual-zone vertical annulus with electroosmosis," *Heliyon*, vol. 9, no. 5, 2023.
- [59] S. I. Abdelsalam and M. Bhatti, "Unraveling the nature of nano-diamonds and silica in a catheterized tapered artery: highlights into hydrophilic traits," *Scientific Reports*, vol. 13, no. 1, p. 5684, 2023.
- [60] M. Bhatti and S. I. Abdelsalam, "Scientific breakdown of a ferromagnetic nanofluid in hemodynamics: enhanced therapeutic approach," *Mathematical Modelling of Natural Phenomena*, vol. 17, p. 44, 2022.
- [61] R. Raza, R. Naz, and S. I. Abdelsalam, "Microorganisms swimming through radiative Sutterby nanofluid over stretchable cylinder: Hydrodynamic effect," *Numerical Methods for Partial Differential Equations*, vol. 39, no. 2, pp. 975-994, 2023.
- [62] S. I. Abdelsalam and A. Zaher, "On behavioral response of ciliated cervical canal on the development of electroosmotic forces in spermatic fluid," *Mathematical Modelling of Natural Phenomena*, vol. 17, p. 27, 2022.
- [63] N. Iftikhar, A. Rehman, H. Sadaf, and M. N. Khan, "Impact of wall properties on the peristaltic flow of Cu-water nano fluid in a non-uniform inclined tube," *International Journal of Heat and Mass Transfer*, vol. 125, pp. 772-779, 2018.
- [64] N. S. Akbar and A. W. Butt, "Ferromagnetic effects for peristaltic flow of Cu–water nanofluid for different shapes of nanosize particles," *Applied Nanoscience*, vol. 6, no. 3, pp. 379-385, 2016.
- [65] T. Elnaqeeb, N. A. Shah, and K. S. Mekheimer, "Hemodynamic characteristics of gold nanoparticle blood flow through a tapered stenosed vessel with variable nanofluid viscosity," *BioNanoScience*, vol. 9, no. 2, pp. 245-255, 2019.